SUPPORTING INFORMATION (SI)

A Programmable DNA Origami Platform for Organizing Intrinsically Disordered Nucleoporins within Nanopore Confinement

Patrick D. Ellis Fisher,[†,‡,§] Qi Shen,[†,‡,§] Bernice Akpinar,[⊥,‖] Luke K. Davis,[‖,▽,O] Kenny Kwok Hin Chung,[†,‡] David Baddeley,[†,‡] Anđela Šarić,[▽,O] Thomas J. Melia,[†] Bart W. Hoogenboom,[‖,▽,O] Chenxiang Lin*[,†,‡] and C. Patrick Lusk*[,†]

[†]Department of Cell Biology, Yale School of Medicine, New Haven, Connecticut 06520, USA

[‡]Nanobiology Institute, Yale University, West Haven, Connecticut 06516, USA

[⊥]Department of Chemistry, Imperial College London, London, SW7 2AZ, UK

[‖]London Centre for Nanotechnology, University College London, 17–19 Gordon Street, London WC1H 0AH, UK

[▽]Department of Physics and Astronomy, University College London, Gower Street, London WC1E 6BT, UK

[O]Institute for the Physics of Living Systems, University College London, Gower Street, London WC1E 6BT, UK

[§]These authors contributed equally to this work; position determined by coin toss.

*Correspondence to: Chenxiang Lin: chenxiang.lin@yale.edu or C. Patrick Lusk: patrick.lusk@yale.edu

Contents:

EXTENDED MATERIALS AND METHODS

DNA origami assembly

DNA origami structures were designed in caDNAno (Figure S1, caDNAno.org) and assembled using an M13mp18 bacteriophage-derived circular ssDNA strand (8064 nt) and oligonucleotides from Integrated DNA Technologies using a 36-hr 85°C–25°C annealing gradient. Structures were purified with rate-zonal centrifugation through a 15–45% glycerol gradient in 1×TE, pH 8.0 (5 mM Tris-Cl, 1 mM EDTA) + 10 mM $MgCl_2$ in an SW 55 rotor (Beckman Coulter) at 50k rpm at 4°C for 1 hr and collecting fractions. Purified DNA origami structures were buffer exchanged into 1×TE + 10 mM $MgCl_2$ and stored at -20°C. ssDNA handles were extended from the 3' end of staple strands at positions indicated in Figure S1. The handle sequences were 5'-AAATTATCTACCACAACTCAC-3' for inner and outer handles and 5'-CGGTTGTACTGTGACCGATTC-3' for biotin functionalization in SMS imaging experiments.

FG-nup expression and purification

FG-domains from *S. cerevisiae* Nsp1 (amino acids 2-603) and Nup100 (amino acids 2-610) were cloned into 10×His-MBP-SUMO-TEV constructs (Figure 1b and Table S1) in a pET-28a-derived vector (Novagen) and expressed in *E. coli* strain BL21-Gold(DE3) (Agilent). Cells were grown in LB medium at 37°C, shaking, until OD = ~0.8, and protein expression was induced with 1 mM IPTG for 4-5hr at 25°C before collection by centrifugation. Cell pellets were stored at -80°C until use, resuspended in lysis buffer (1×PBS, pH 7.4 [137 mM NaCl, 2.7 KCl, 11.8 mM NaH_2PO_4], 0.5 mM TCEP, 0.1 mM PMSF, 1× Roche cOmplete protease inhibitors), and lysed in a cell disruptor. Whole cell lysates were spun at 35k rpm for 45min in a Type 45 Ti rotor (Beckman Coulter) and supernatant was decanted and filtered through a 0.45 μm cellulose acetate membrane. The resulting filtered lysate was spiked with 0.1% Tween 20 and 25mM imidazole, and applied to a 5 mL HisTrap column (GE) on an ÄKTA system (GE) at a flow rate of 1 mL/min. The column was washed with wash buffer (1×PBS, 0.1% Tween 20, 25 mM imidazole) and eluted on a gradient of elution buffer (1×PBS, 0.1% Tween 20, 500 mM imidazole). Protein concentration was determined by BCA assay (Pierce). Eluate was spiked with 10% glycerol, flash frozen in liquid N_2, and stored at -80°C until use.

Maleimide-DNA preparation

5'-labeled amino-DNA oligonucleotides were purchased from IDT, resuspended in deionized H_2O, and buffer exchanged into 10 mM HEPES, pH 7.4 using a Micro Bio-spin 6 column (Bio-Rad) to remove free amines. Sulfo-SMCC (Pierce and G-Biosciences) was resuspended in de-ionized H_2O at 50°C. 2 mM sulfo-SMCC was reacted with 200 μM amino-DNA for 3–5.5hr at 37°C in 100 mM HEPES, pH 7.4, and purified by ethanol precipitation. Dried maleimide-DNA pellets were stored at -20°C until use.

Protein-DNA conjugation

Maleimide-DNA pellets (above) were resuspended in 10 mM HEPES, pH 7.4 and mixed with affinity purified FG-nups in PBS-TG buffer (1×PBS, 0.1% Tween 20, 10% glycerol) at a final concentration of 250 μM maleimide-DNA and 50 μM FG-nup (5:1). This reaction was incubated at 37°C for 3–5.5hr, then stored at 4°C overnight. Excess DNA was purified away from conjugated proteins using size exclusion chromatography on a Superdex Increase 10/300 column (GE Healthcare) at a flow rate of 0.15 mL/min in PBS-TG buffer. Conjugation efficiency was verified by SDS-PAGE using Coomassie or SYPRO Red stain (Thermo Fisher).

Hybridization of FG-nups to DNA origami

DNA-conjugated FG-nups were added to DNA origami rings at 7.5× excess over the number of handles (e.g. 5 nM origami × 48 handles × 7.5 = 1.8 μM FG-nup-DNA) in PBS-TG + 10 mM $MgCl_2$ and incubated for 3hr at 37°C. Hybridization reactions were purified by rate-zonal centrifugation, as described in purifying the origami, through a 15–45% glycerol gradient in the hybridization buffer. The purified product is called a NuPOD (NucleoPorins Organized on DNA).

SDS-AGE and SDS-PAGE

For SDS-agarose gel electrophoresis (SDS-AGE), 1.5% agarose gels were made with and run in running buffer (0.5×TBE [44.5 mM Tris, 44.5 mM boric acid, 1 mM EDTA], 10 mM $MgCl_2$, 0.05% SDS). Gels were run at 60V for 3hr, SDS was removed by shaking the gel in H_2O. Gels were then stained with 0.5 μg/mL ethidium bromide (EtBr) and destained for 10min in H_2O before scanning for EtBr with a Typhoon gel scanner (GE Healthcare).

For SDS-polyacrylamide gel electrophoresis (SDS-PAGE), bis-Tris, pH 6.5, 8% acrylamide gels were loaded with samples boiled in Laemmli buffer and run in MOPS-SDS buffer (50 mM Tris, 50 mM MOPS, 1 mM EDTA, 0.1% SDS) at 200V for 1hr. Gels were stained using Coomassie or SYPRO Red stain (Thermo Fisher, following manufacturer's instructions).

Quantification of FG-nups on NuPODs

For purified NuPODs, DNA origami concentration was determined using ethidium bromide staining on SDS-AGE (after removal of SDS from gel), compared to known concentrations of DNA origami. Immunoblots were run with either equivalent NuPOD concentration (equal DNA origami, different amounts of protein) or equal protein concentration (different amounts of DNA origami, equal DNA handle number). SDS-PAGE gels were run as above, and transferred to nitrocellulose membranes at 100V for 1hr in transfer buffer (25 mM Tris, 192 mM glycine, 0.1% SDS, 20% methanol). Membranes were washed in TBS-T buffer (25 mM Tris, 150 mM NaCl, 0.05% Tween 20, pH 7.5), labeled with an αPentaHis-HRP conjugate (Qiagen), and developed with standard western blot enhanced chemiluminescence reagents (Pierce). A concentration curve of MBP-Nup100, run on the same blot, was fit in GraphPad Prism to a quadratic curve and was used to interpolate total moles of protein, which was then divided by moles of DNA origami to convert to copy number per NuPOD.

Coarse-grained molecular dynamics simulations

MD simulations were performed using a combination of an *NVE* (constant number of particles *N*, constant volume *V*, constant energy *E*) time integration algorithm and a Langevin thermostat, with the LAMMPS package (version 5 Nov 2016).[1]

The DNA origami ring was modeled as an open cylinder comprised of neighboring spheres with diameter = 2.0 nm and arranged as to mimic the experimental setup, with the sphere centers positioned along a cylinder of radius 23.9 nm and height 9.0 nm, and of a radius of 29.9 nm and height 11.5 nm for the inside and outside grafted NuPODs, respectively. The cylinder was kept fixed throughout the simulation and was excluded from the integration scheme. The DNA linkers were modelled as stiff chains of beads with diameter = 2.2 nm, connected by harmonic springs (stiffness 1000 k_BT /nm^2) and angular potential (stiffness 1000 k_BT /rad^2) between nearest-neighbors. The linkers were kept fixed at one end at specific points along the inner cylindrical wall, as defined by the respective NuPOD configurations, and were free to rotate around that anchor. The FG-nup proteins were modelled as beads-on-a-chain[2,3] connected by harmonic springs with stiffness 1000 k_BT /nm^2, where each bead, with diameter = 0.76 nm, corresponded to two amino acids, a choice that yielded the correct persistence length for FG-nups. Individual FG-nup polymers had one end attached to the tip of a DNA linker rod *via* a stiff harmonic spring. MBP at its other end was modelled as a sphere with a diameter of 4.83 nm to match its approximate absolute volume (PBD ID: 1OMP);[4,5] it was attached to the free-end of the FG-Nup polymer *via* a harmonic spring (stiffness 1000 k_BT /nm^2).

The ring, DNA linker rods, FG-nup polymers and MBP all experienced excluded-volume (short-range repulsive) interaction, implemented through a truncated and shifted repulsive Lennard Jones potential, $U^{rep}(r) = 4\varepsilon_{LJ}\left[\left(\frac{\sigma_{ij}}{r}\right)^{12} - \left(\frac{\sigma_{ij}}{r}\right)^{6}\right] + \varepsilon_{LJ}$ for $r < 2^{1/6}\sigma_{ij}$ and zero elsewhere, with r the center-to-center distance between particles i and j with respective diameters d_i and d_j, and $\sigma_{ij} = \frac{1}{2}\left(d_i + d_j\right)$. ε_{LJ} was set to 500 k_BT. In addition, an attractive FG-nup polymer-polymer (pp) interaction was implemented with a roughly exponential decay (dropping to zero at a center-to-center distance of ${r_c}^{att} = 2\sigma_{ij} = 2d_i = 1.56$ nm here) with strength ε_{pp} (in units of k_BT) at contacts between the beads making up the FG-nups. Specifically, the attractive potential was based on $U^{att}(r) = -\varepsilon_{pp}\exp\left(-\frac{r-\sigma_{ij}}{\lambda}\right)$, with $\lambda = \sigma_{ij} = d_i = 0.76$ nm here, shifted and truncated to yield a total pair potential for the polymer beads of the form $U_{pp}(r) = U^{rep}(r) - \varepsilon_{pp}$ for $r < 2^{1/6}\sigma_{ij}$; $U_{pp}(r) = U^{att}(r) - U^{att}(r = {r_c}^{att}) - (r - {r_c}^{att})\left(\frac{d\,U^{att}(r)}{dr}\right)_{r={r_c}^{att}}$ for $2^{1/6}\sigma_{ij} \le r < {r_c}^{att}$; and zero elsewhere.

The phenomenological parameter ε_{pp} was set through a comparison of MD polymer brush simulations and experimental thickness data of FG-nup films, following a procedure previously applied by Zahn, *et al.*[2] (Figure S6), which yielded $\varepsilon_{pp} = 0.41\ k_BT$ for Nsp1 and $\varepsilon_{pp} = 0.45\ k_BT$ for Nup100, for the here chosen shape of the interaction potential.

All simulations were equilibrated for 7×10^6 timesteps (roughly equivalent to 48 μs) and a further 8×10^6 timesteps (~54 μs) were used for data analysis. Each simulation was run 5 times with different initial conditions and random seeds to verify equilibration and to obtain reliable statistical sampling.

Size measurement by Dynamic Light Scattering

Dynamic light scattering (DLS) measurements were performed using a Wyatt DynaPro Nanostar instrument (Wyatt Technology) at room temperature. NuPODs were diluted 5 times in 1×PBS, pH 7.4, 16 mM $MgCl_2$. The data was collected with a 663.8 nm laser at a power setting of 50%. Peak radius cutoffs were fixed according to a range from 1 to 300 nm. The data were analyzed using Dynamics 7.1.7 software by performing a regularization fit using a sphere model.

Single-Molecule Switching (SMS) Microscopy

Immunolabeled NuPODs were attached to coverslips *via* BSA-biotin/streptavidin binding, through biotinylated anti-handles (see Figure S1), and mounted in custom-made sealed chambers,[6] filled with 10 mM MEA, 20 mM Na_2SO_3 and 16 mM $MgCl_2$ in PBS with 50% glycerol. Samples were labeled with Alexa 647 (Thermo Fisher)-conjugated secondary antibodies and imaged under widefield epi-fluorescence illumination (642 nm laser at ~40 kW/cm^2) at 50-100 Hz (Andor Zyla 4.2 sCMOS camera) for approximately 15 minutes to generate a single dataset. An activation laser (405 nm at < 0.3 kW/cm^2) was started at around 10 min. Fluorescent beads (yellow-green, 200 nm, Thermo Fisher)[7] were imaged in the Alexa 647 channel as fiducial markers for drift correction.

Image data analysis: STORM data was both acquired and analyzed with PYthon Microscopy Environment (PYME; http://www.python-microscopy.org/). Individual blinking events were localized using an sCMOS specific weighted least-squares fit with a 2D Gaussian model.[8] Localizations with precision less than 17 nm were discarded. STORM images were rendered using the jittered triangulation method[7] and individual NuPODs were segmented by choosing a threshold such that 90% of the total signal was contained within the segmented objects. To ensure only images of single NuPODs of high quality were analyzed, structures which failed to meet the following criteria were rejected: 1) a minimum of 100 localization events, 2) less than 200 nm in diameter, 3) measured circularity between 0.75 and 1. NuPOD images were fitted with a model of a ring convolved with a 2D Gaussian (σ = 17 nm)[9] to provide a measurement of the radius.

Preparation of lipid vesicles for supported lipid bilayers

The preparation of supported lipid bilayers largely followed procedures described elsewhere.[10] 1,2-dihexadecanoyl-*sn*-glycero-3-phosphocholine (DPPC; zwitterionic head group) and Dimethyldioctadecylammonium Bromide Salt (DDAB; cationic head group) were purchased from Avanti Polar Lipids (Alabaster, AL). The two lipids dissolved in chloroform were mixed to a molar ratio of 3:1 (DPPC:DDAB). Next, the solvent was slowly evaporated by passing a steady stream of nitrogen in a fume hood for 1 hr and then placing under vacuum for at least 4 h. The dry lipid film was resuspended in MilliQ water to a

concentration of ~1 mg/ml and was transferred to bath sonicator (Fisher Scientific, Loughborough, UK), maintained ~15^{o}C above the gel-liquid transition temperature (~41 ^{o}C and ~45 ^{o}C for DPPC and DDAB, respectively) of the constituent lipids. The large multilamellar vesicles were disrupted by 15 min sonication treatments at frequencies between 37 and 80 kHz. The solution containing the lipid dispersion was loaded into an Avanti mini-extruder kit (Avanti Polar Lipids) and kept above the gel-liquid transition temperature of the lipids at all times. The lipid solution was forced through a polycarbonate filter (GE Healthcare Lifesciences, Buckinghamshire, UK) with a 100 nm nominal pore diameter and the extrusion process repeated at least 20 times to yield small unilamellar vesicles.

AFM sample preparation

2 µl of the small unilamellar vesicles (prepared as described above) along with 1 µl 1M $MgCl_2$, 1 µl 1M $CaCl_2$ and 16 µl of MilliQ water were deposited onto a freshly cleaved mica disc. The disc was placed in a humid chamber and heated to 65^{o}C for 10 minutes before slowly cooling to room temperature over 20 minutes. This process induced vesicle rupture and yielded a positively charged, gel-phase supported lipid bilayer (SLB). Excess vesicles in the supernatant were removed by rinsing first with water and then exchanged with buffer (10 mM PB, 26 mM $MgCl_2$ pH 7.0). The rinsing process was gently repeated three to five times to ensure a clean and uniform surface before addition of 2-4 µl of NuPODs (~2-5 nM) prior to imaging.

Control experiments were conducted to evaluate the interaction strength between the nups and the underlying substrate. 1 µl of 100 nM protein-DNA solution was added to a freshly cleaved mica disc or SLB and left to equilibrate for ~20 minutes before imaging in buffer (as before).

AFM imaging and analysis

All AFM measurements were performed in liquid. Images of 48×MBP(in/out) NuPODs in Figure 4d were collected using a Multimode 8 AFM with E-scanner (Bruker, Santa Barbara, CA) in PeakForce Tapping mode with an amplitude of 10 nm at 4 kHz. For these measurements a Biolever mini (Bruker) cantilever was used, with a resonance frequency of 25 kHz in water and spring constant of 0.1 N/m. All other images were obtained using a FastScan Bio AFM (Bruker) operated in tapping mode, using FastScan Ds (Bruker) cantilevers driven near their resonance frequency of ~110 kHz in water, at an amplitude of 10~20 nm. The force applied to the sample was minimized by setting the highest possible amplitude set-point that allowed an accurate tracing of the DNA origami rings. This was typically above 85% of free oscillation as measured ~100 nm above the sample surface. With the measured cantilever spring constant of 0.15 N/m, this implies maximum interaction forces of the order of 0.1 nN (presuming a strongly damped cantilever oscillation close to the sample surface, such that the maximum force is approximately given by the change in the amplitude multiplied by the spring constant).

While the supported DPPC:DDAB bilayers provided an adequate passivation of the AFM substrate (Figure S9), they bound the NuPODs only loosely: At imaging speeds exceeding the ones used here, the scanning probe readily dislodged the NuPODs in our experiments. Single line scanning experiments, e.g. used in earlier high-

speed AFM experiments,[11] provided an enhanced time resolution whilst minimising disturbance to the NuPODs and also tracing the DNA origami ring as a reliable reference structure against which to gauge variations of the conjugated proteins.

AFM images were processed using zeroth order background plane subtraction and first-order line-by-line flattening to remove height offset and sample tilt in the Nanoscope Analysis software (Bruker).

SI REFERENCES

1. Plimpton, S. Fast Parallel Algorithms for Short-Range Molecular Dynamics. *J. Comput. Phys.* 1995, 117, 1-19.
2. Zahn, R.; Osmanovic, D.; Ehret, S.; Araya Callis, C.; Frey, S.; Stewart, M.; You, C.; Görlich, D.; Hoogenboom, B. W.; Richter, R. P. A Physical Model Describing the Interaction of Nuclear Transport Receptors with FG Nucleoporin Domain Assemblies. *eLife* 2016, 5.
3. Osmanovic, D.; Bailey, J.; Harker, A. H.; Fassati, A.; Hoogenboom, B. W.; Ford, I. J. Bistable Collective Behavior of Polymers Tethered in a Nanopore. *Phys. Rev. E* 2012, 85, 061917.
4. Sharff, A. J.; Rodseth, L. E.; Spurlino, J. C.; Quiocho, F. A. Crystallographic Evidence of a Large Ligand-Induced Hinge-Twist Motion between the Two Domains of the Maltodextrin Binding Protein Involved in Active Transport and Chemotaxis. *Biochemistry* 1992, 31, 10657-10663.
5. Voss, N. R.; Gerstein, M. 3V: Cavity, Channel and Cleft Volume Calculator and Extractor. *Nucleic Acids Res.* 2010, 38, W555-562.
6. Lin, C.; Jungmann, R.; Leifer, A. M.; Li, C.; Levner, D.; Church, G. M.; Shih, W. M.; Yin, P. Submicrometre Geometrically Encoded Fluorescent Barcodes Self-Assembled from DNA. *Nat. Chem.* 2012, 4, 832-839.
7. Baddeley, D.; Cannell, M. B.; Soeller, C. Visualization of Localization Microscopy Data. *Microsc. Microanal.* 2010, 16, 64-72.
8. Lin, R.; Clowsley, A. H.; Jayasinghe, I. D.; Baddeley, D.; Soeller, C. Algorithmic Corrections for Localization Microscopy with sCMOS Cameras - Characterisation of a Computationally Efficient Localization Approach. *Opt. Express* 2017, 25, 11701-11716.
9. Szymborska, A.; de Marco, A.; Daigle, N.; Cordes, V. C.; Briggs, J. A.; Ellenberg, J. Nuclear Pore Scaffold Structure Analyzed by Super-Resolution Microscopy and Particle Averaging. *Science* 2013, 341, 655-658.
10. Leung, C.; Hodel, A. W.; Brennan, A. J.; Lukoyanova, N.; Tran, S.; House, C. M.; Kondos, S. C.; Whisstock, J. C.; Dunstone, M. A.; Trapani, J. A.; Voskoboinik, I.; Saibil, H. R.; Hoogenboom, B. W. Real-Time Visualization of Perforin Nanopore Assembly. *Nat. Nanotechnol.* 2017, 12, 467-473.
11. Viani, M. B.; Pietrasanta, L. I.; Thompson, J. B.; Chand, A.; Gebeshuber, I. C.; Kindt, J. H.; Richter, M.; Hansma, H. G.; Hansma, P. K. Probing Protein-Protein Interactions in Real Time. *Nat. Struct. Biol.* 2000, 7, 644-647.

SUPPORTING FIGURES S1–S14, TABLES S1–S2

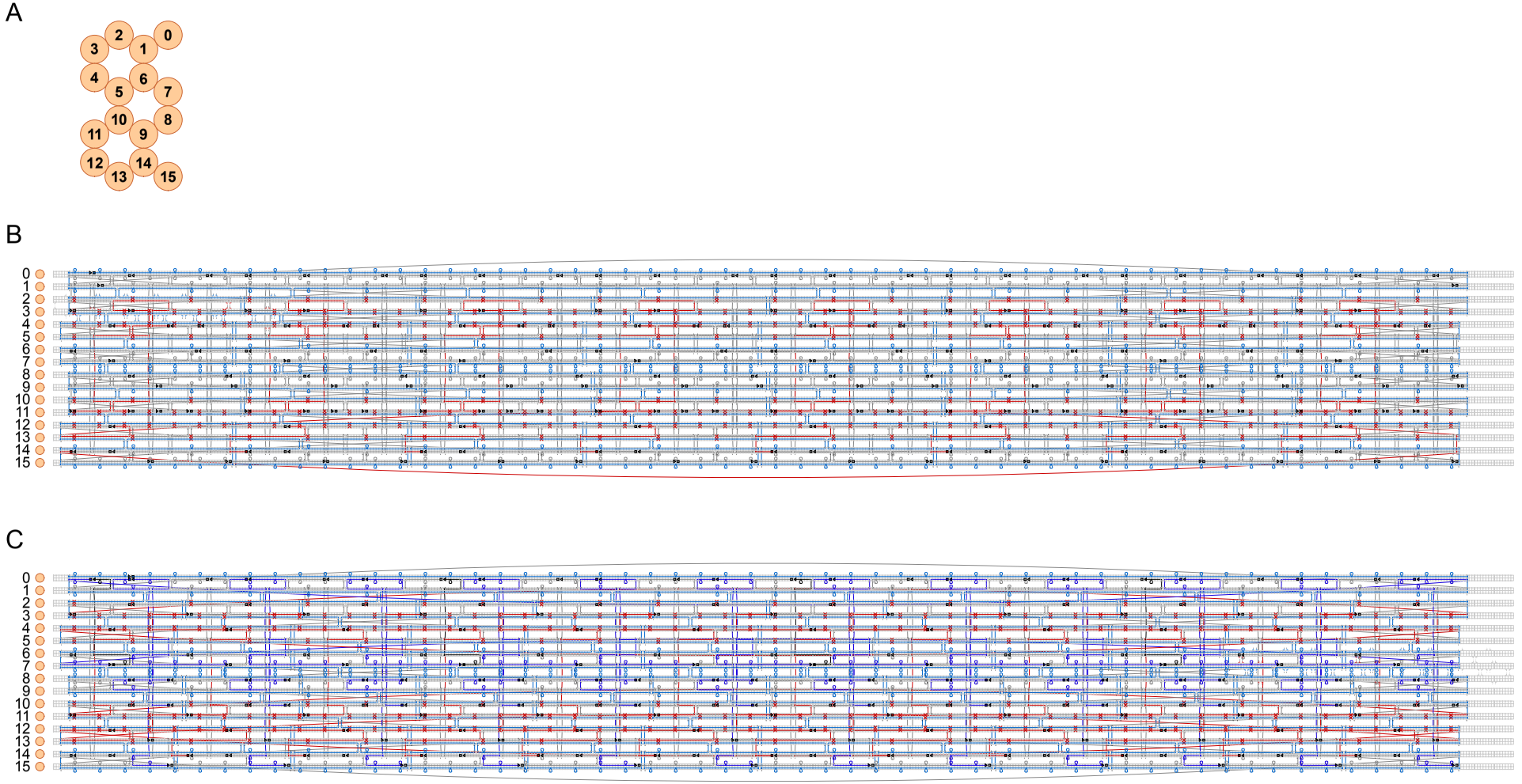

Figure S1. DNA origami designs, rendered in caDNAno. Cross section view (a, *cf*. Figure 1a) and strand diagrams for the (b) 0–32 inner handle NuPOD, and (c) 48 inner handle NuPOD and 48 outer handle NuPOD. Scaffold strand is in blue. Staples for inner handles are shown in red, outer handles in dark blue. Handle positions for biotinylated DNA anti-handles (for SMS imaging experiments) are in black.

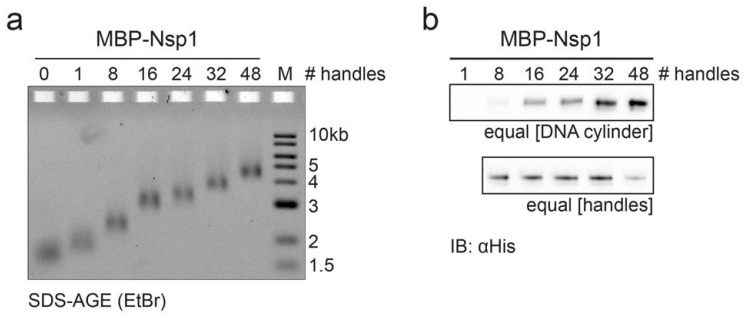

Figure S2. Mobility shift assay and immunoblots of MBP-Nsp1 NuPODs. (a) Step-wise mobility shift of NuPODs as the number of FG-domains increases (MBP-Nsp1; M, molecular weight marker; SDS-agarose, EtBr stain; *cf*. Figure 2a). (b) Immunoblots (αHis) loaded with either equal amount of DNA cylinders or number of DNA handles (*cf*. Figure 2b).

Fig. S3 A

MBP-Nup100(in)

handles

1

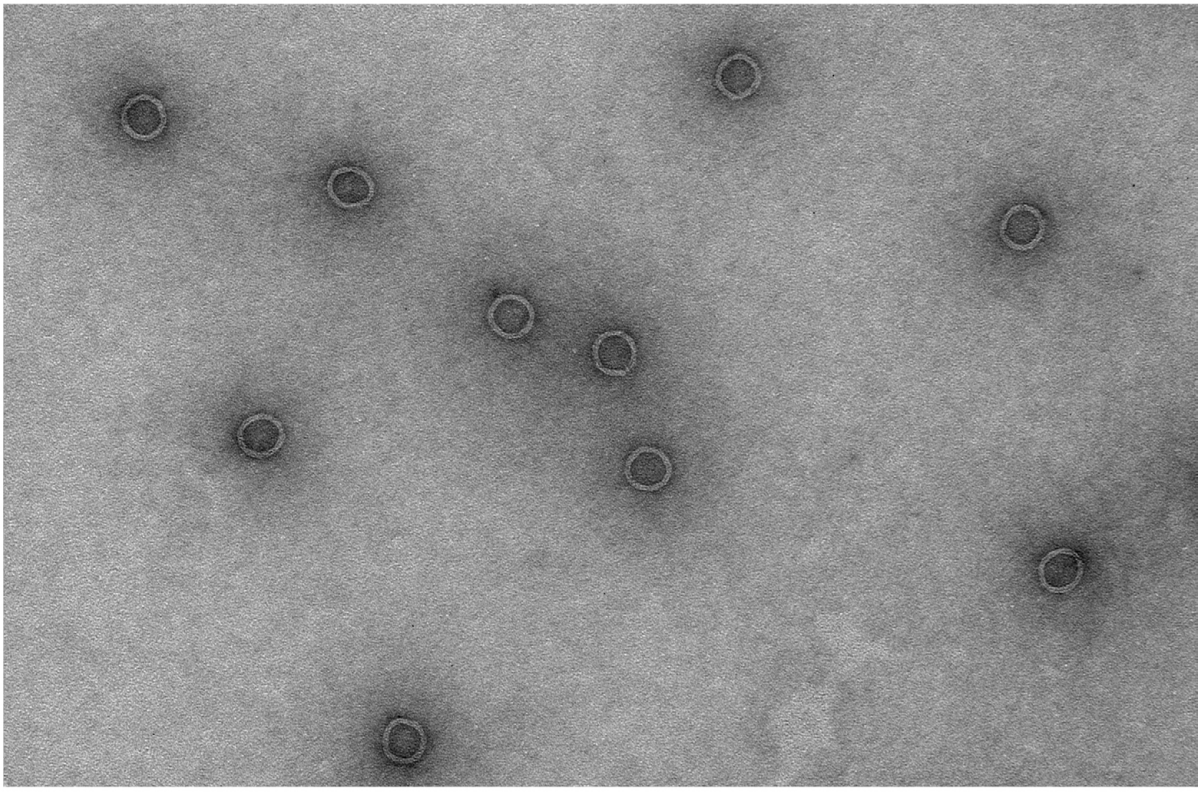

8

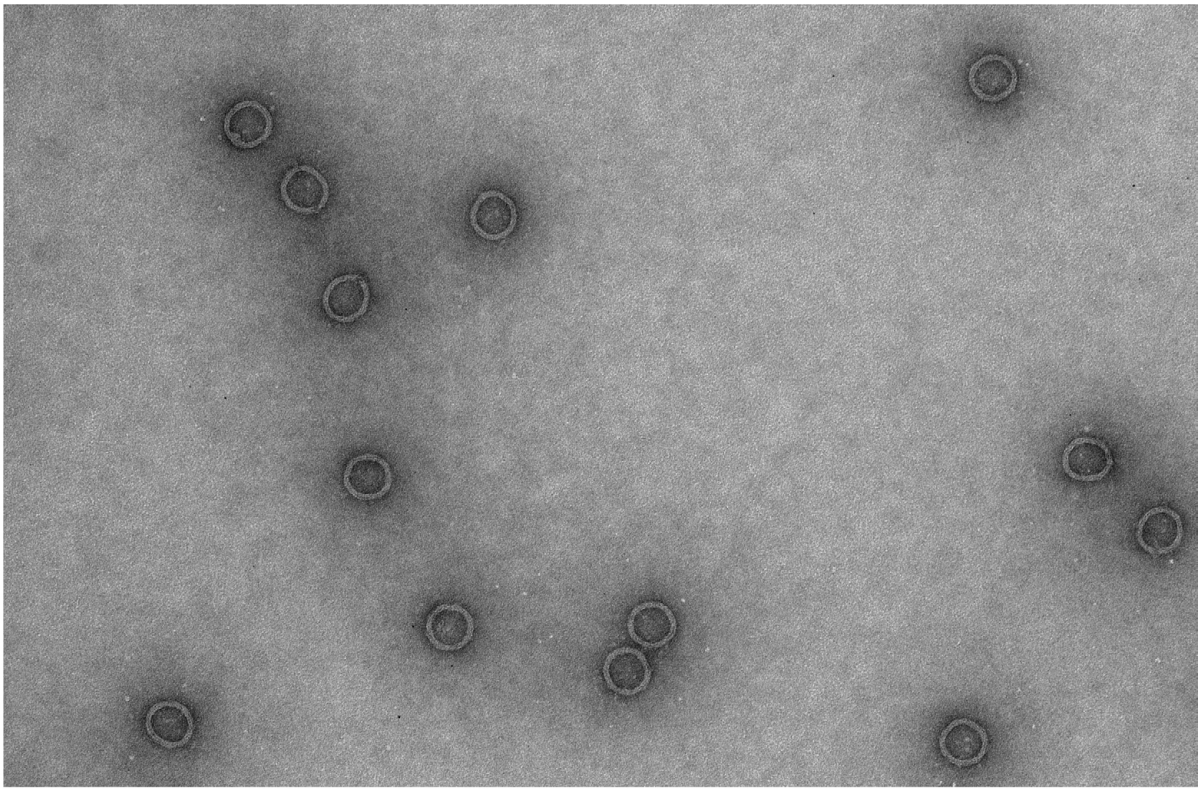

100 nm

Fig. S3 B

MBP-Nup100(in)

handles

16

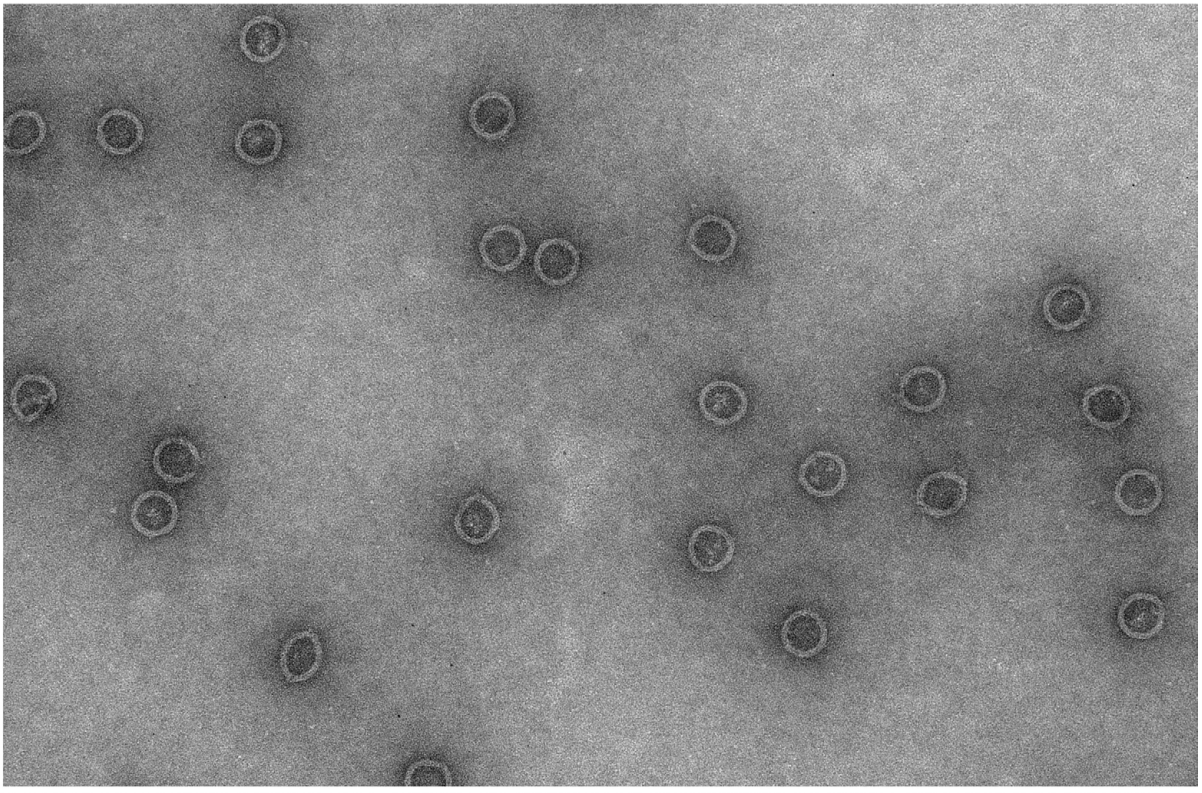

24

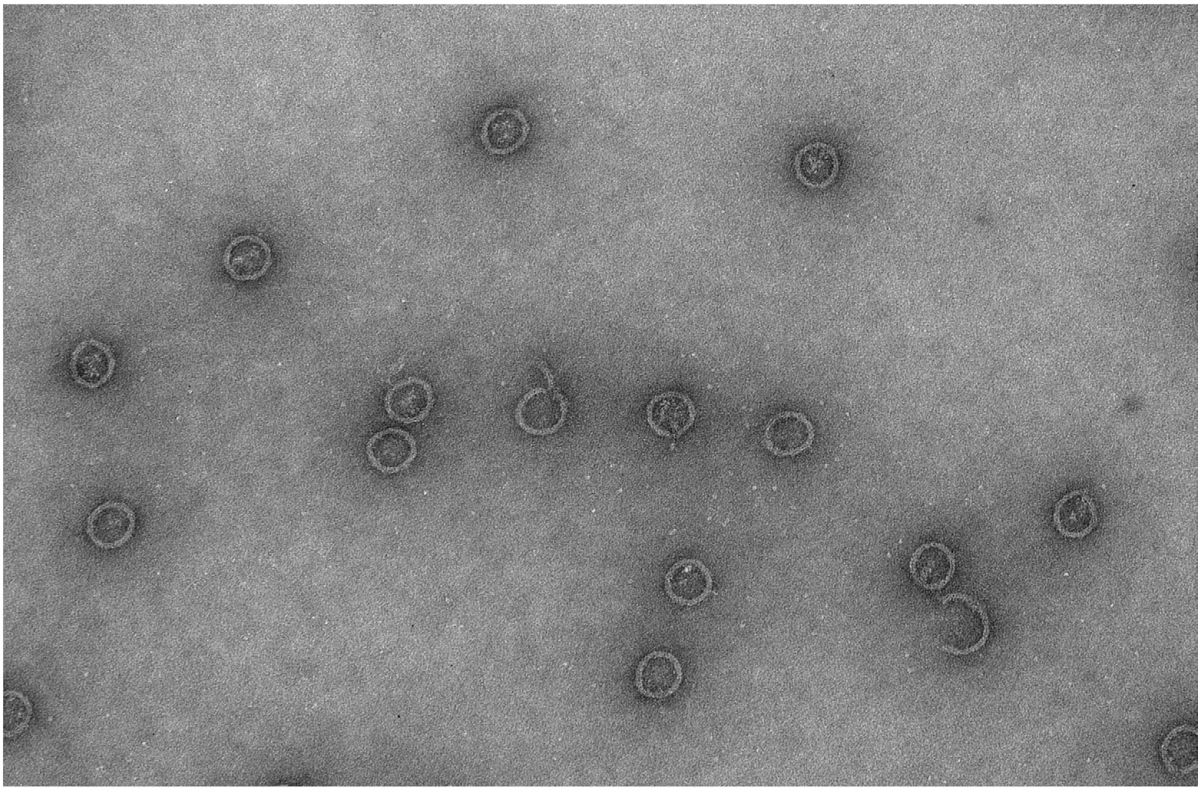

100 nm

Fig. S3 C

MBP-Nup100(in)

handles

32

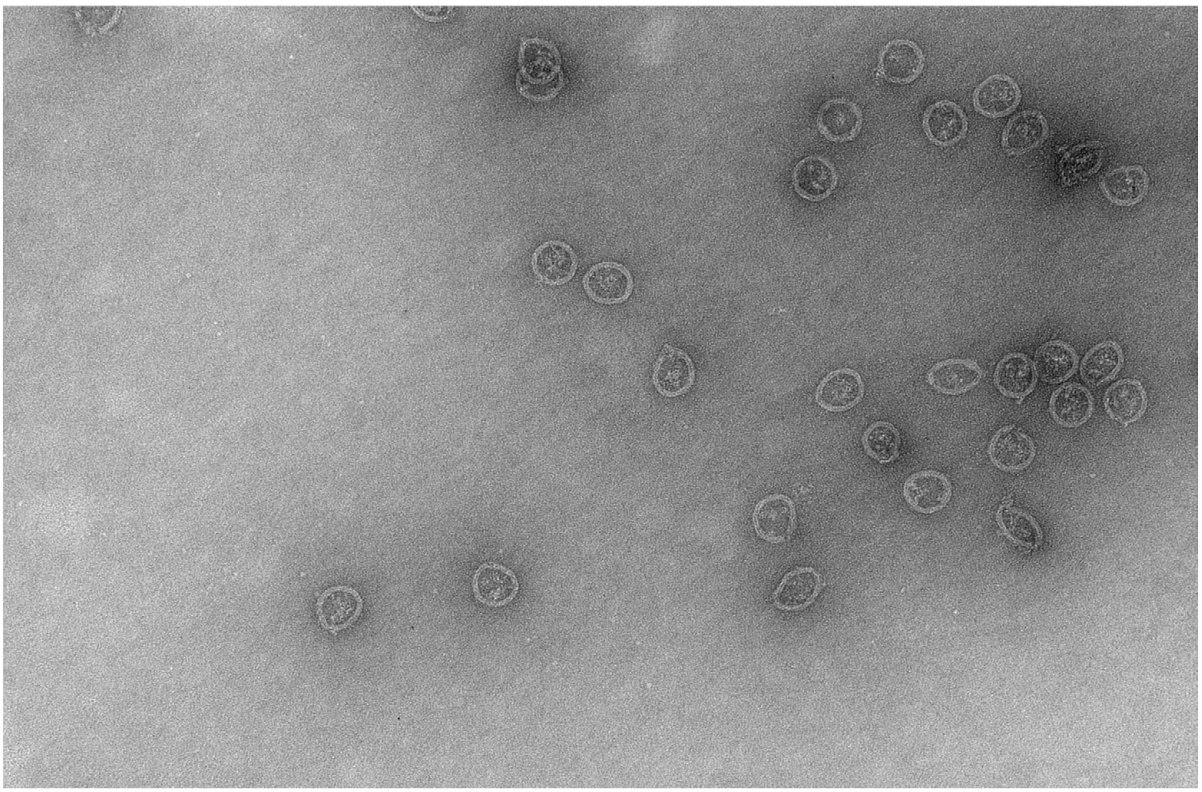

48

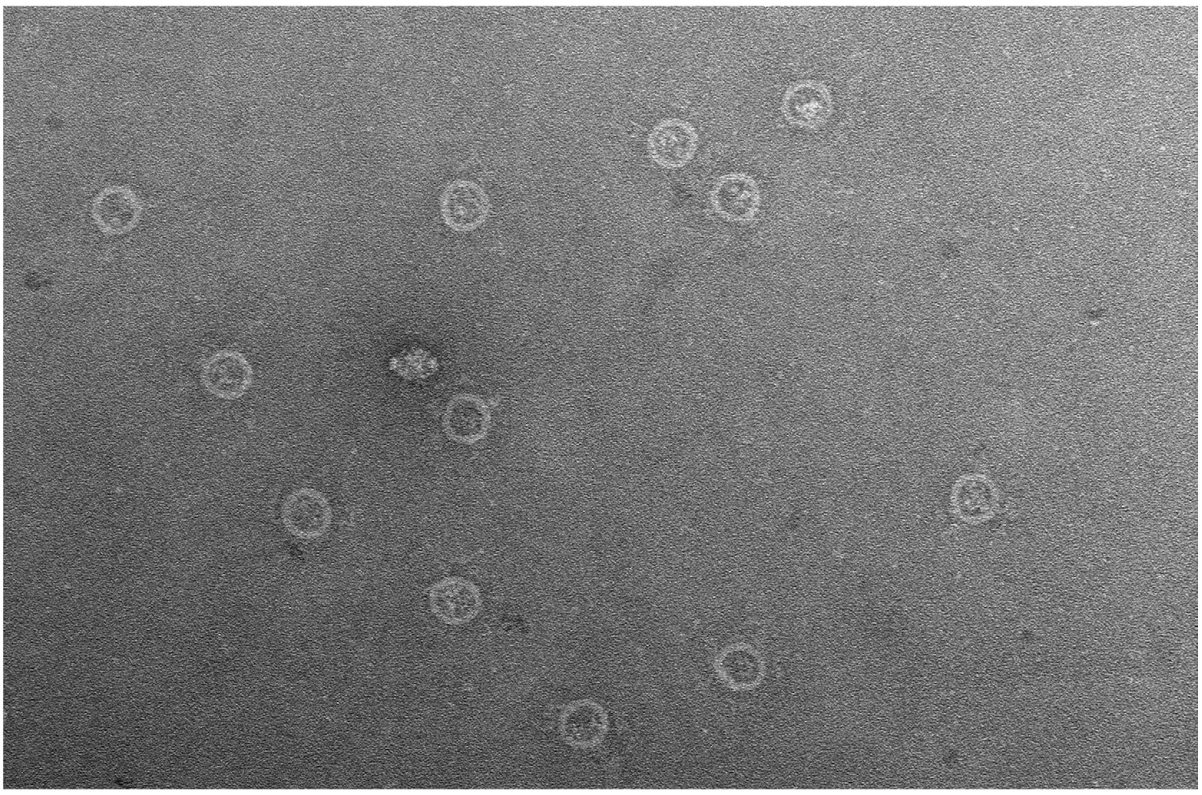

100 nm

Fig. S3 D
MBP-Nup100
handles

48
out

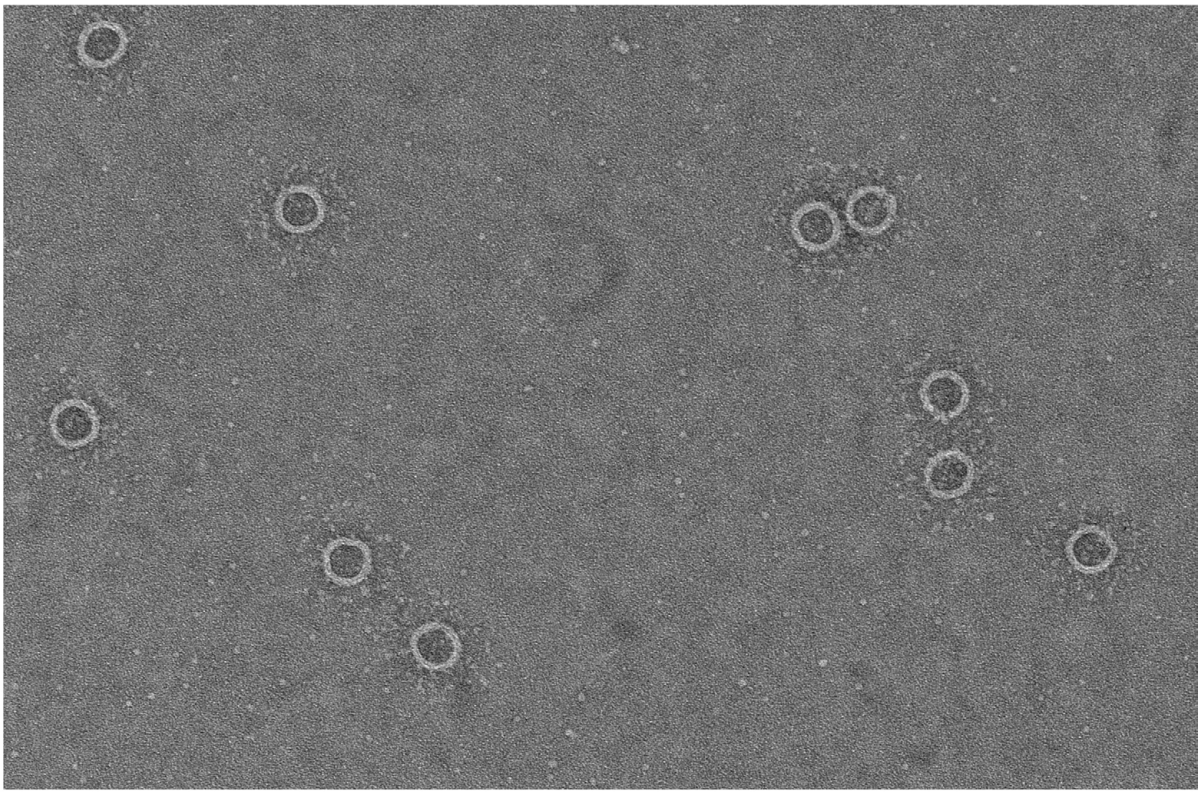

Figure S3. Morphology of MBP-Nup100 NuPODs. Full TEM images of n×MBP-Nup100(in), n = 1, 8 (a), 16, 24 (b), 32, 48 (c), and 48×MBP-Nup100(out) (d).

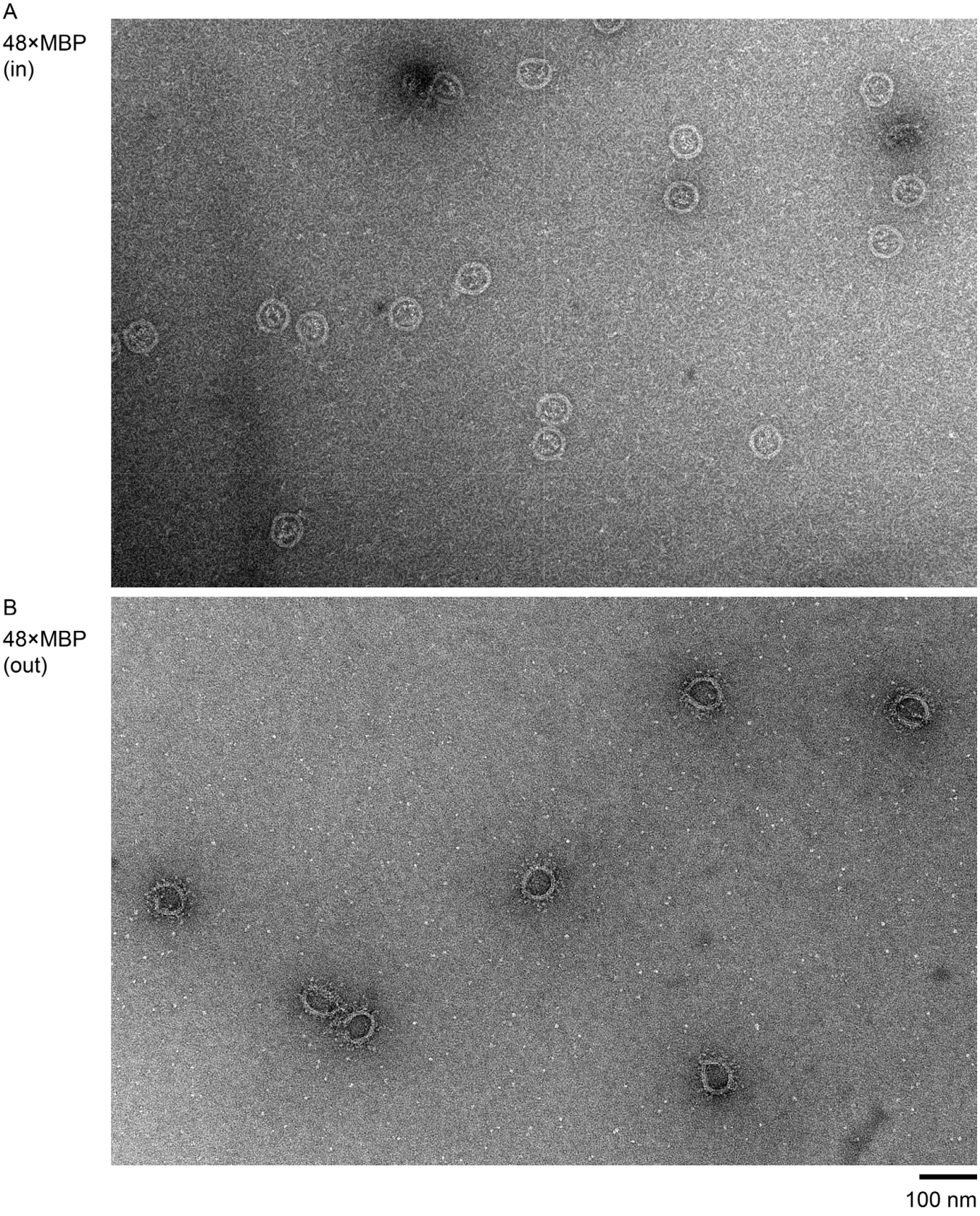

Figure S4. Morphology of MBP NuPODs. Full TEM images of 48×MBP(in) (a) and 48×MBP(out) (b).

Fig. S5 A

MBP-Nsp1(in)

handles

1

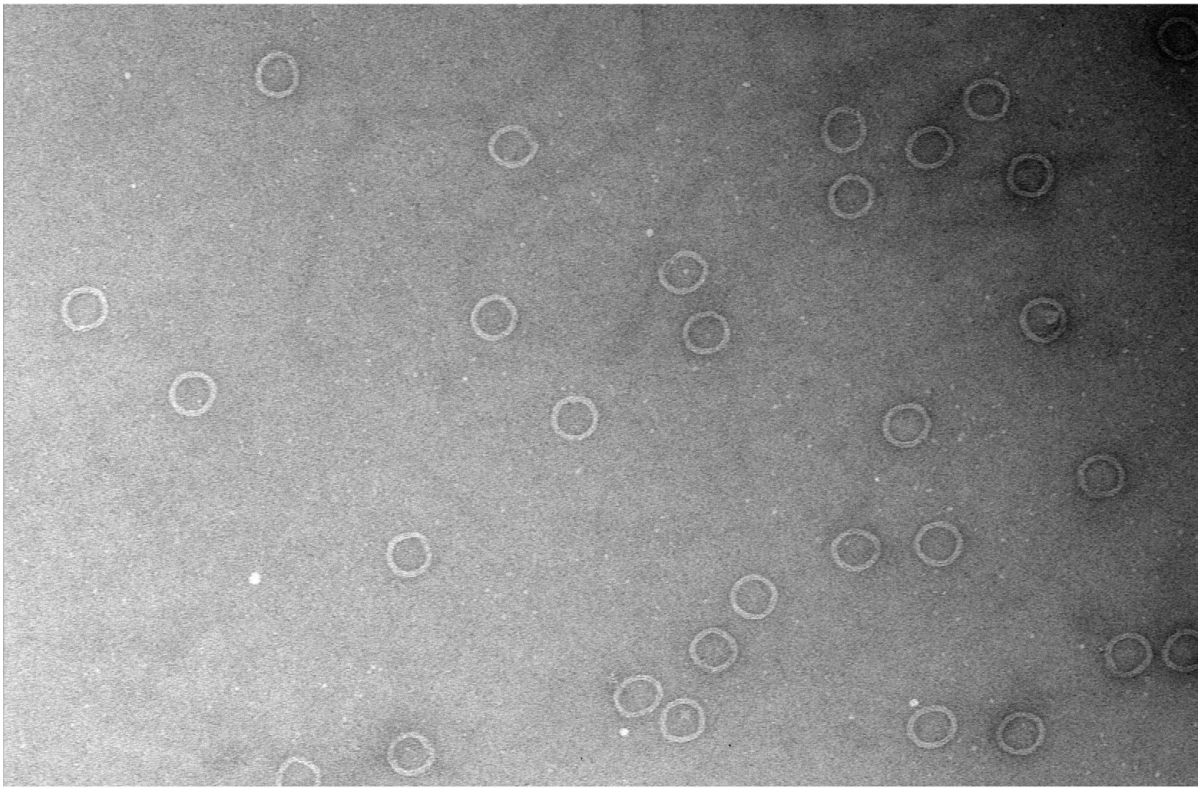

8

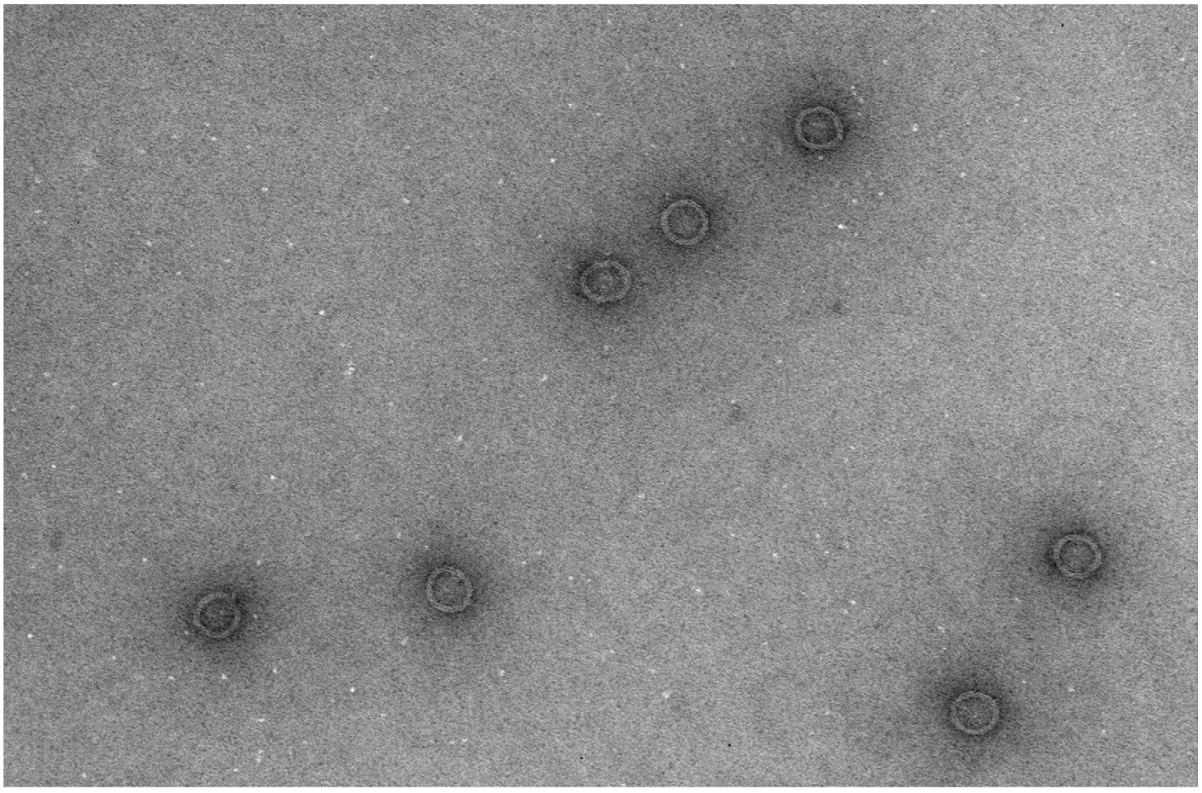

100 nm

Fig. S5 B

MBP-Nsp1(in)

handles

16

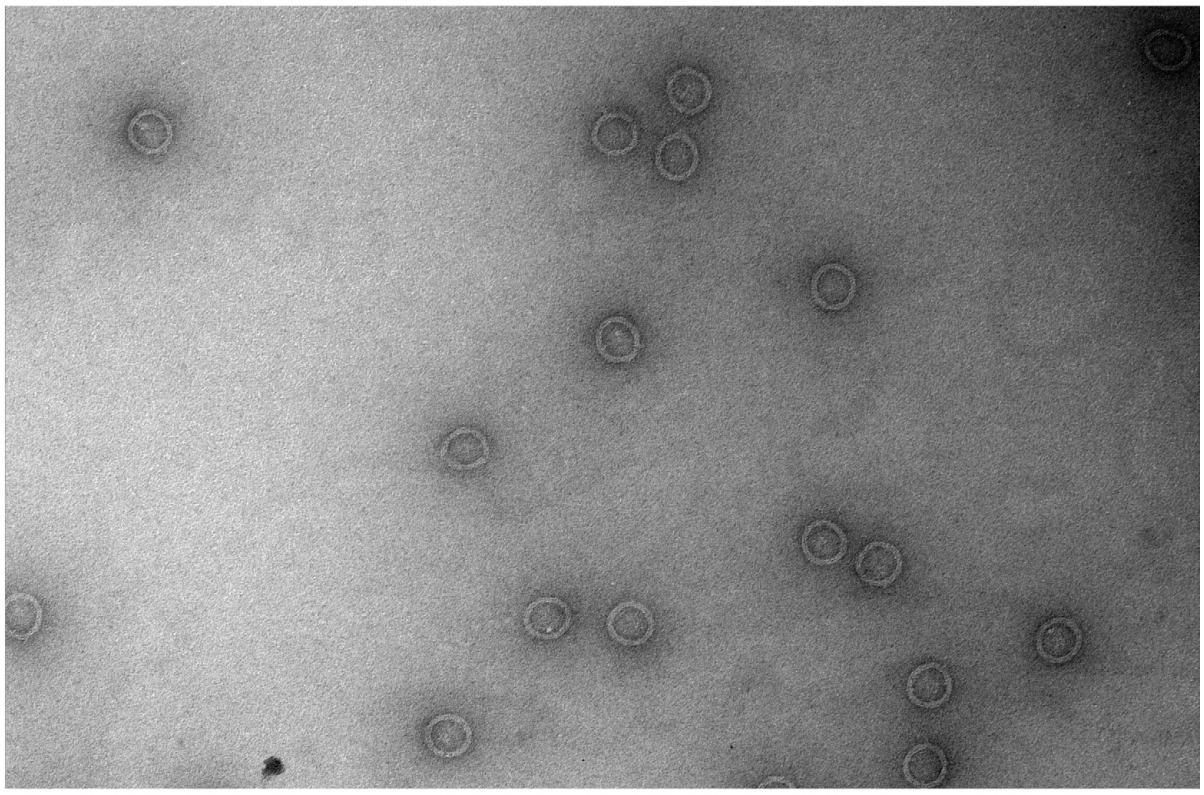

24

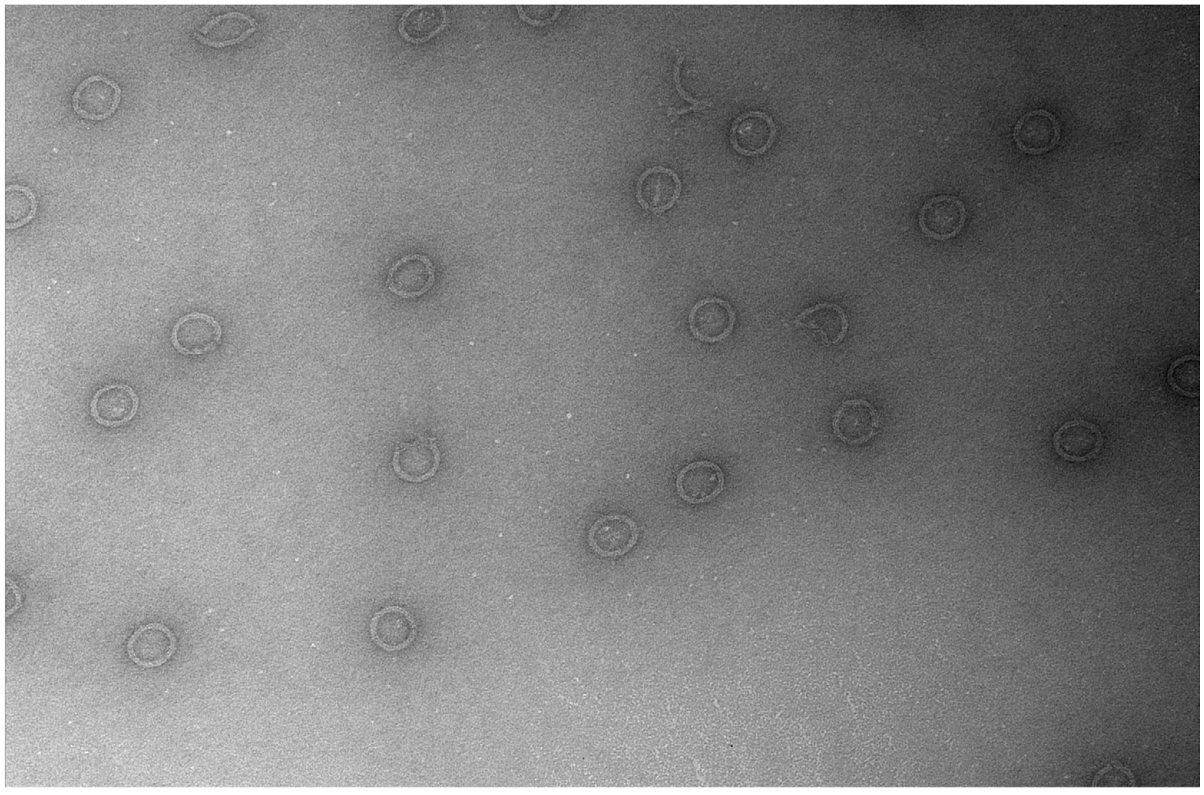

100 nm

Fig. S5 C

MBP-Nsp1(in)

handles

32

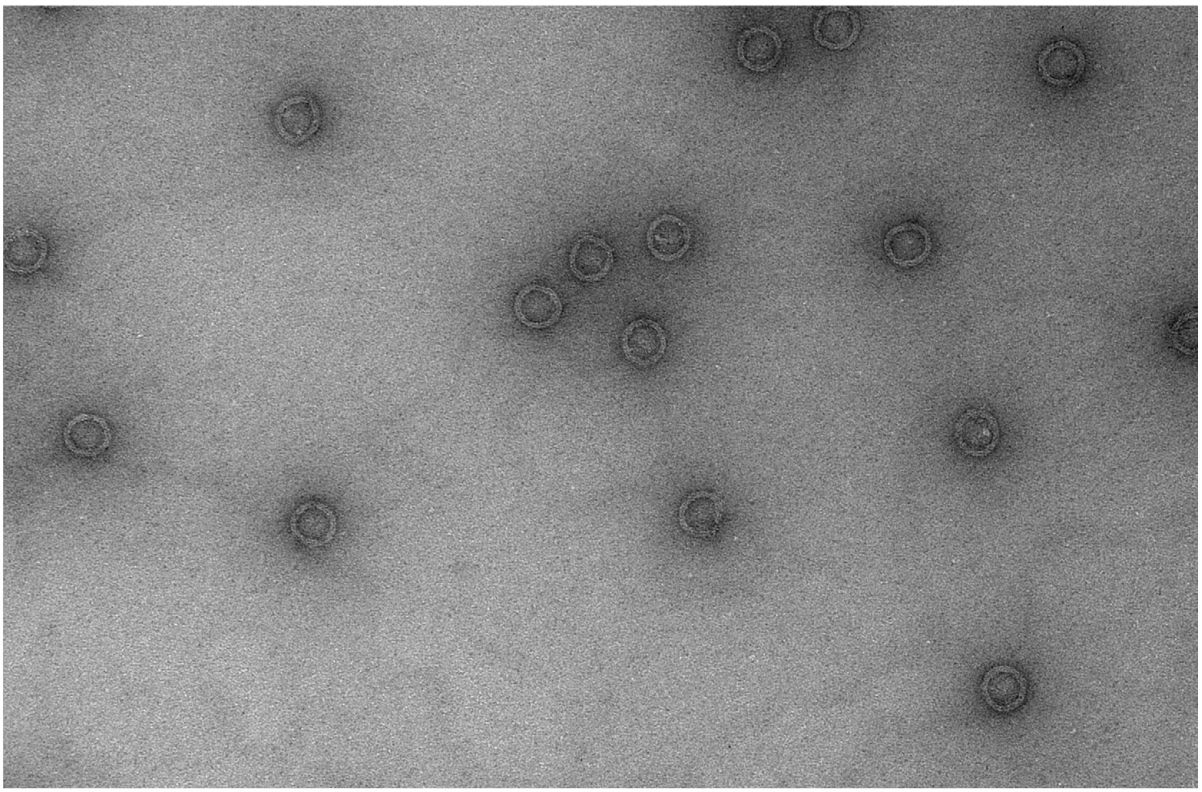

48

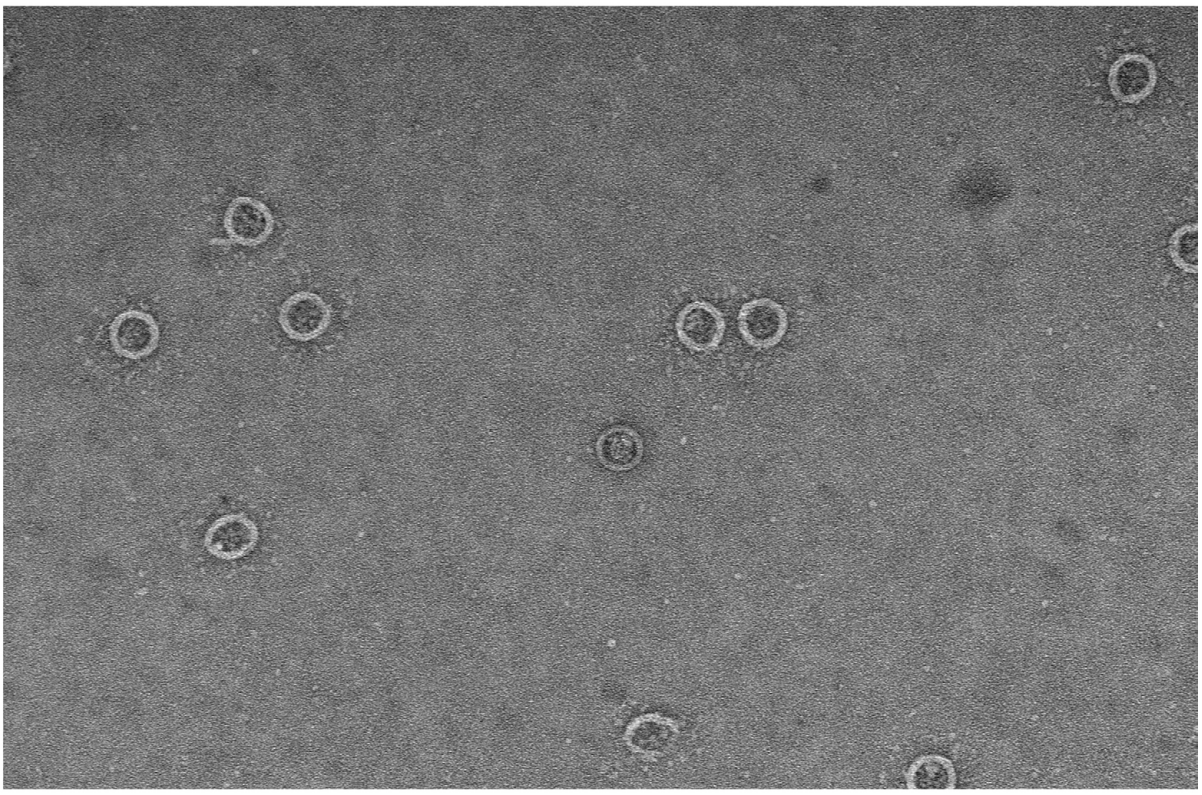

100 nm

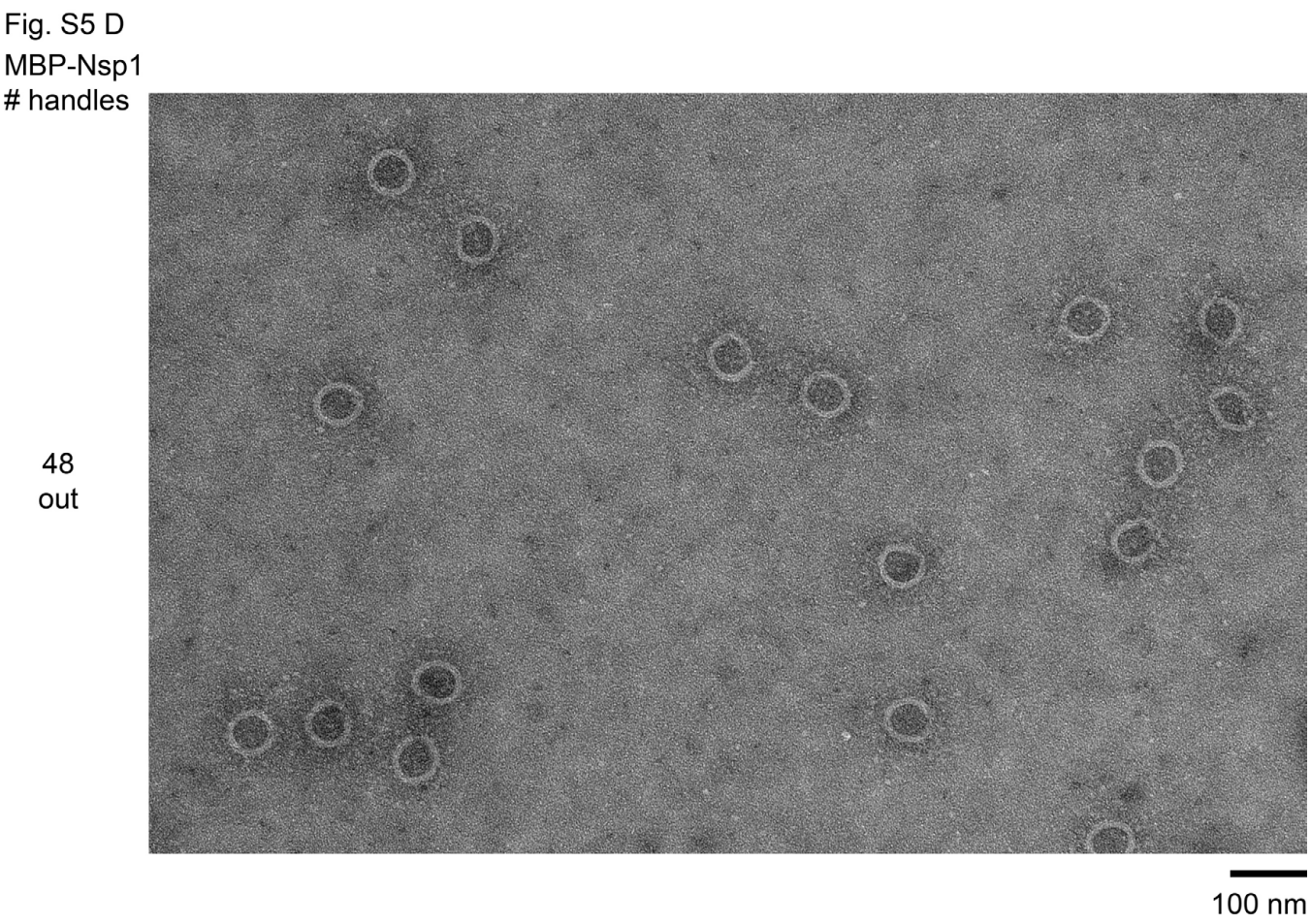

Figure S5. Morphology of MBP-Nsp1 NuPODs. Full TEM images of n×MBP-Nsp1(in), n = 1, 8 (a), 16, 24 (b), 32, 48 (c), and 48×MBP-Nsp1(out) (d).

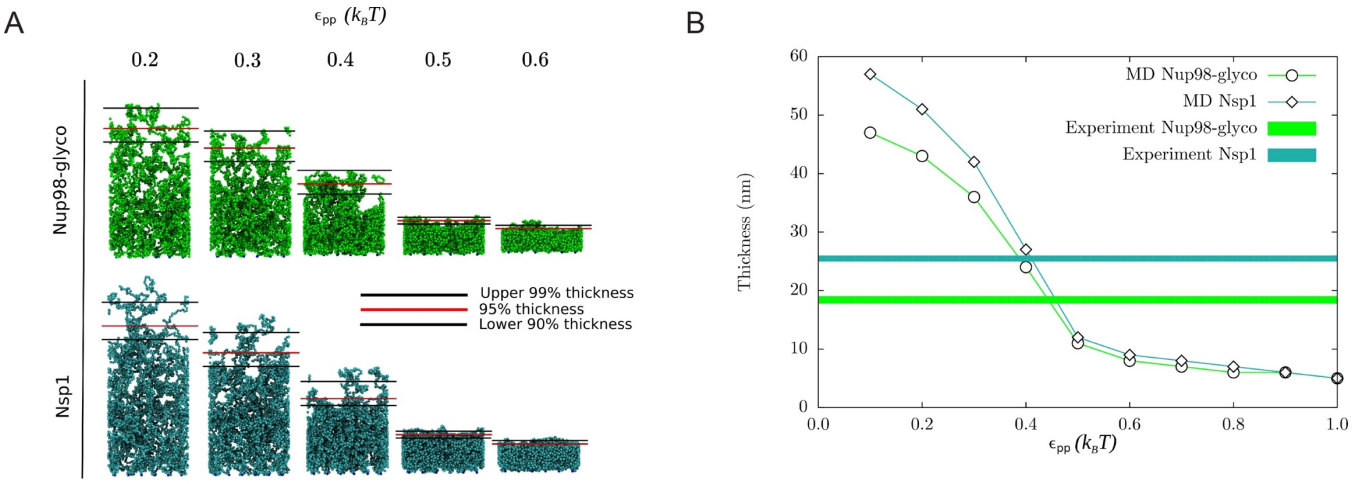

Figure S6. MD parameter settings for attractive interactions between Nup100 and Nsp1. (a) Snapshots of equilibrated molecular dynamics simulations of FG-nup polymer assemblies grafted in a planar geometry, with periodic boundary conditions along the in-plane coordinate axes. The grafting density was set at 5.5 pmol/cm^2 (i.e., 3.3 molecules per 100 nm^2) to replicate the conditions that applied for the experimental data used here to calibrate the inter-bead affinity parameter ε_{pp}, following Zahn, *et al*. [2]. Given the available data, glycosylated Nup98 was used to calibrate ε_{pp} for its *S. cerevisiae* orthologue Nup100. MD snapshots are shown for ε_{pp} = 0.2, 0.3, 0.4, 0.5, 0.6 k_BT. Horizontal bars mark the film thicknesses set by the thresholds corresponding to 90%, 95% and 99% of the total beads. (b) Film thickness (95% threshold) for these assemblies as a function of the inter-bead affinity ε_{pp}, compared with the experimental data (horizontal lines) for the corresponding FG-nup films.[2] The phenomenological interaction energy ε_{pp} is about an order of magnitude larger than in previous calculations,[2] because of the shorter range of the inter-bead attraction that has been assumed here (described in SI extended methods).

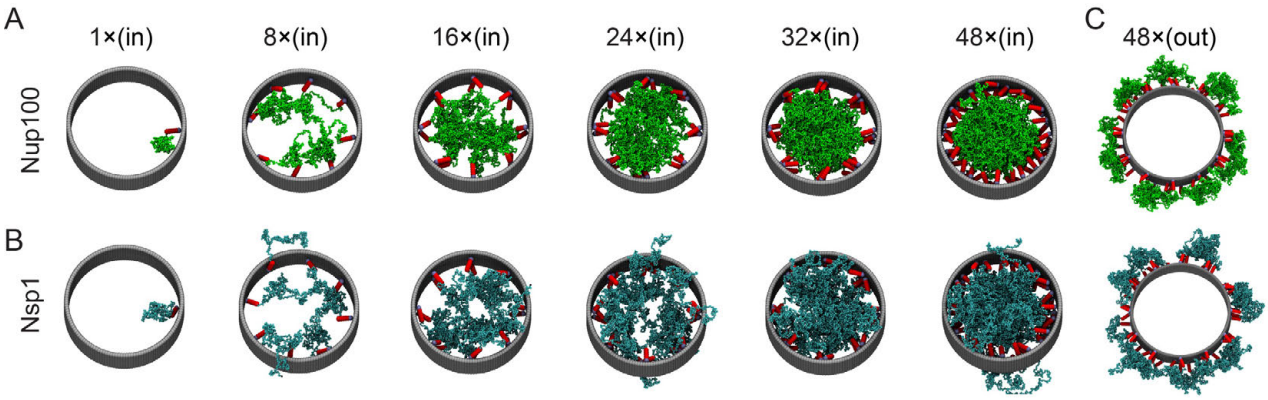

Figure S7. Snapshots of equilibrated molecular dynamics simulations of NuPODs with the MBP termination removed. (a) For n×Nup100(in), with n = 1, 8, 16, 24, 32 and 48. (b) As *A*, for Nsp1. (c) For 48×Nup100(out) and 48×Nsp1(out).

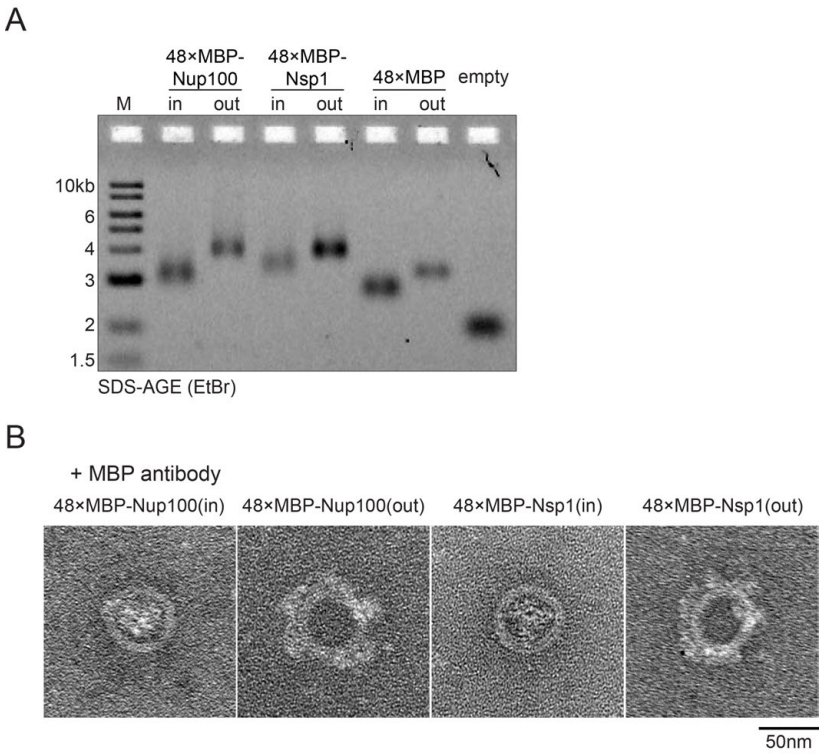

Figure S8. Analysis of NuPOD (in) vs. (out) varieties. (a) SDS-AGE (EtBr stain) showing mobility shifts between different NuPOD constructs. NuPODs with proteins grafted outside run slower than their inside-grafted counterparts. All protein-containing NuPODs run more slowly than the empty DNA origami cylinder. (b) MBP antibody-induced protein collapse in NuPODs. TEM of NuPODs after binding to MBP antibody for SMS microscopy experiments.

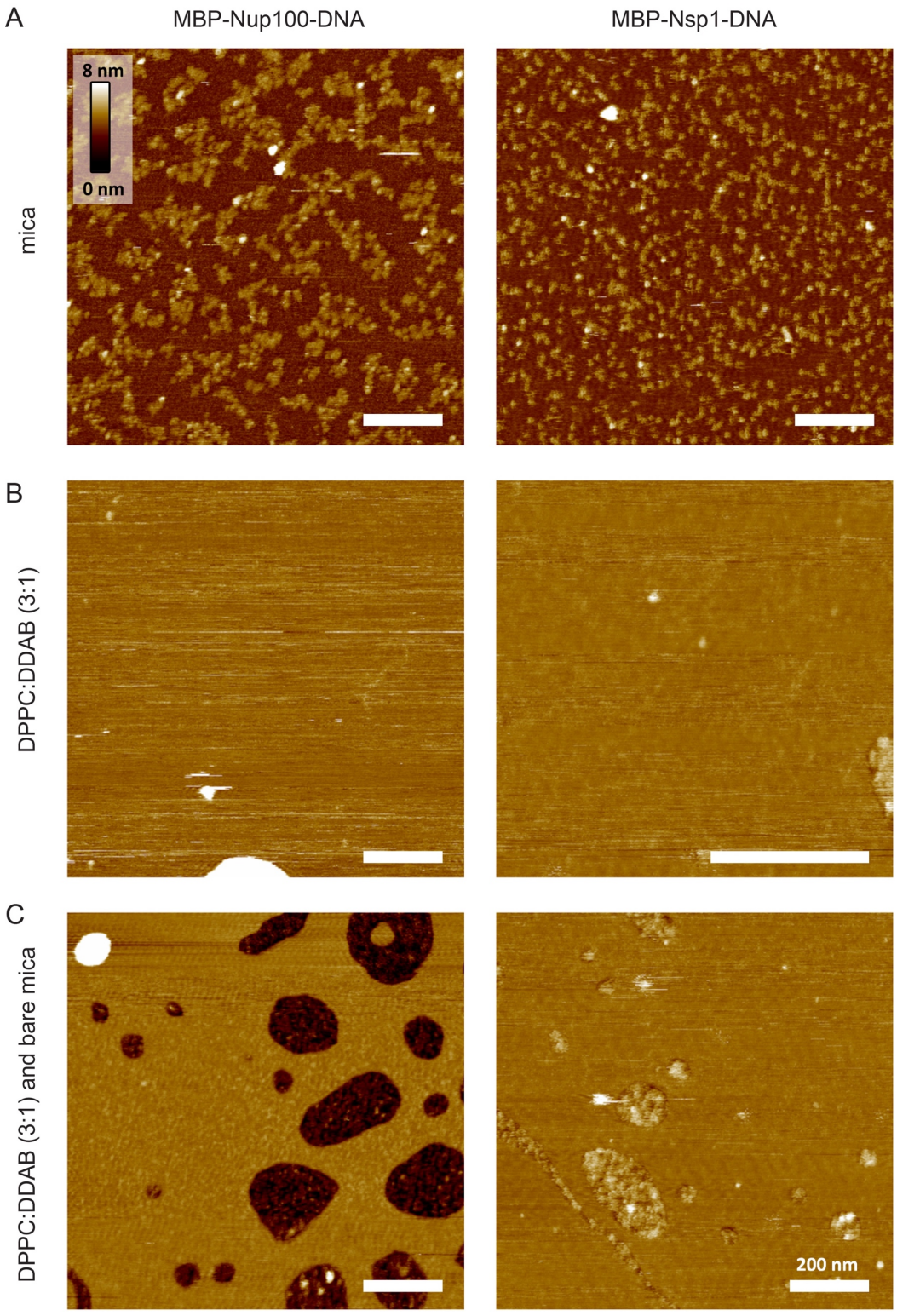

Figure S9. AFM topographs of protein-DNA conjugates on mica and on supported lipid bilayers. (a) On a cleaved mica surface, as commonly used for AFM, both MBP-Nup100-DNA and MBP-Nsp1-DNA readily adsorb under the conditions used in our experiments (see SI extended methods). (b) A supported DPPC:DDAB (3:1) bilayer effectively passivates the mica substrate, showing practically no adsorption of protein (under otherwise identical conditions). (c) When the mica substrate is only partially covered by the lipid bilayer, proteins adsorb and/or aggregate on the exposed mica surface only, while the bilayer surface remains free of protein.

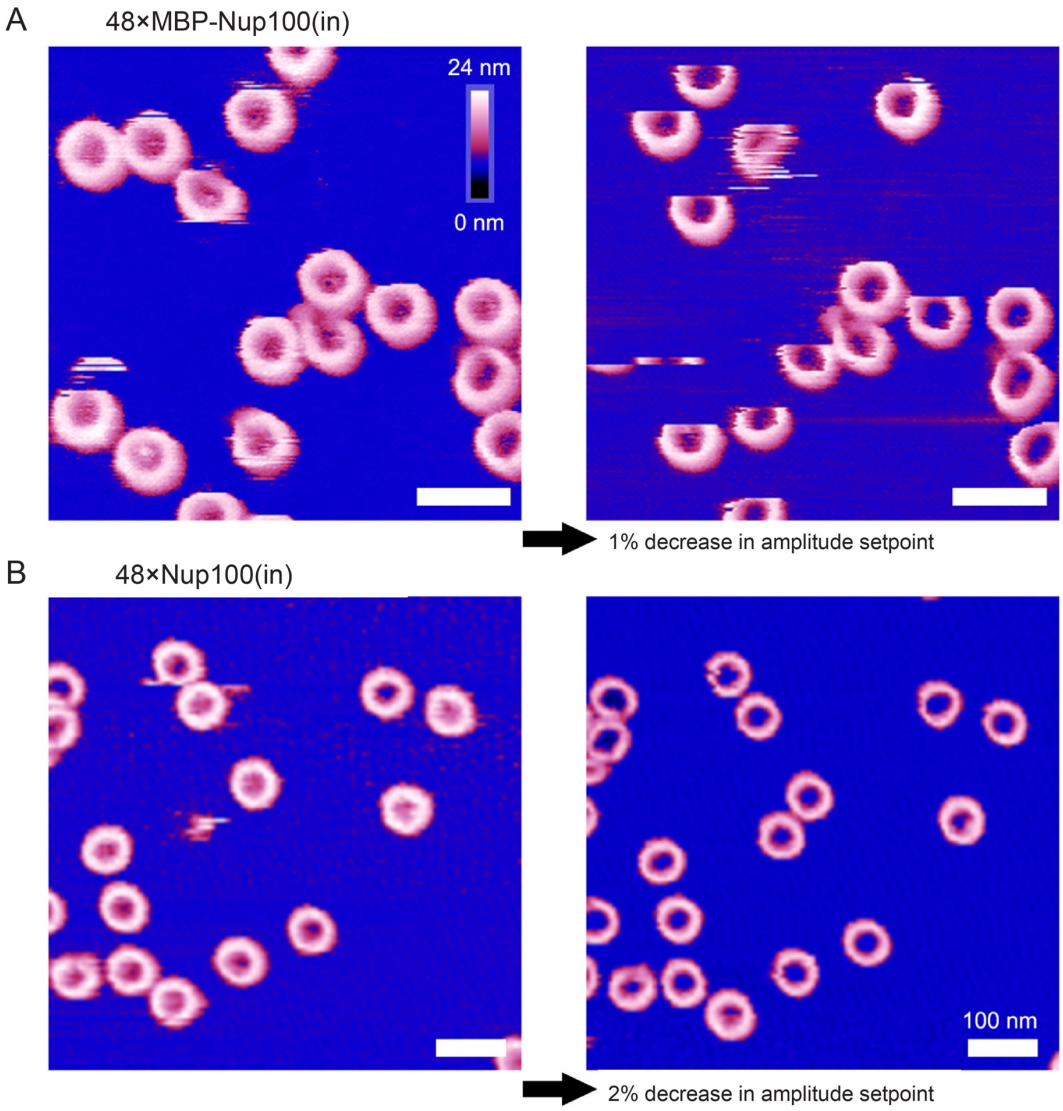

Figure S10. AFM Imaging of NuPODs illustrating that the appearance of the NuPOD lumen can strongly depend on the applied force. In tapping mode AFM—as applicable here—the amplitude setpoint determines the tip-sample interaction and is a compromise between the need to minimize invasiveness (i.e., requiring a high setpoint, close to the free amplitude of the AFM probe as measured just above the surface) and the need to detect surface features with sufficient signal-to-noise ratio (*a priori* requiring a lower setpoint). (a) Imaging of the same area with 48×MBP-Nup100(in) NuPODs, recorded at an amplitude of ~15 nm, for optimized parameter settings (left) and for an only marginally reduced setpoint (right). The optimum parameter range was rather narrow, and minor changes in setpoint (~1%) could change the appearance of proteins in the NuPOD lumen. (b) As in a, for 48×Nup100(in) with MBP cleaved off.

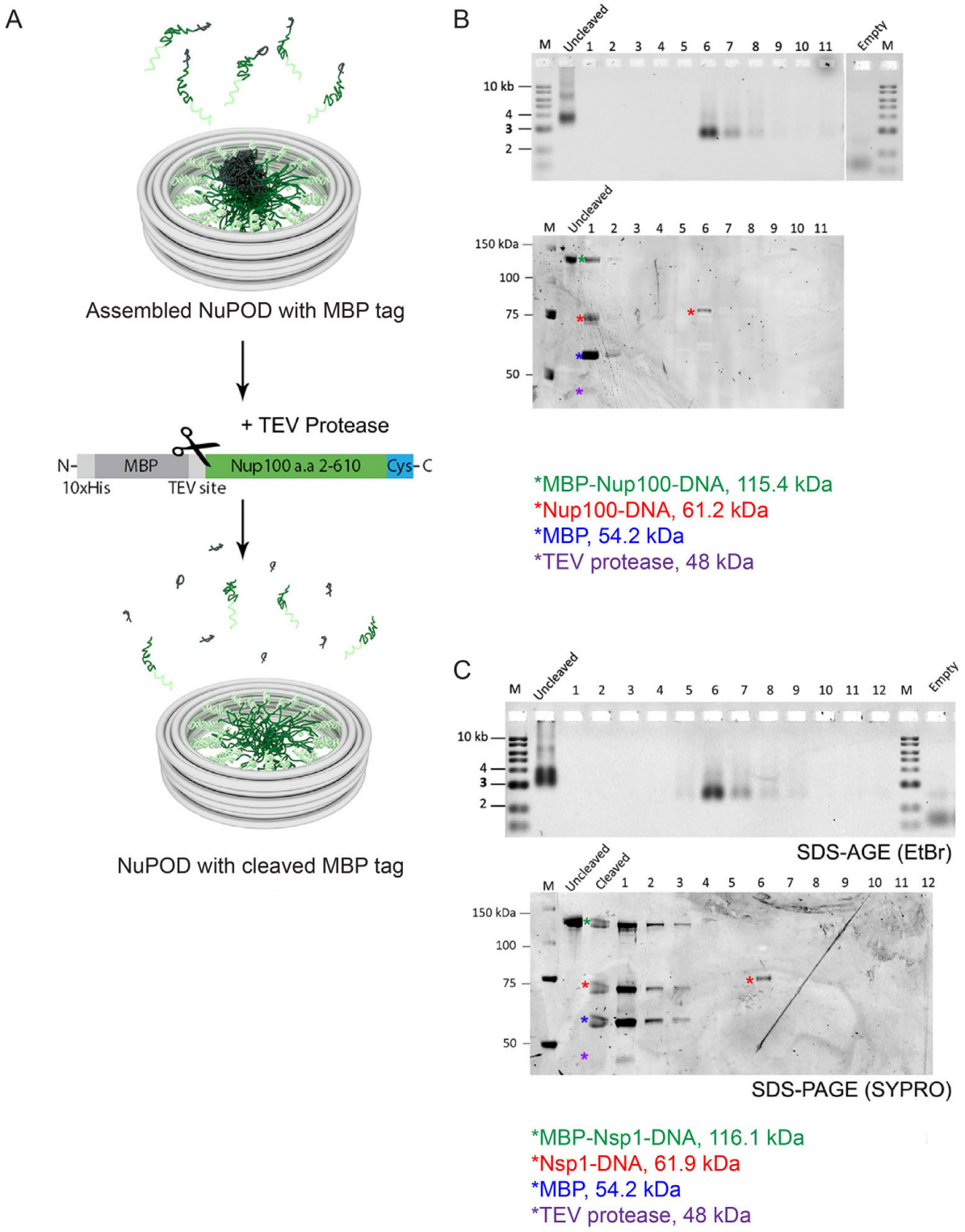

Figure S11. Removal of the MBP tags from NuPODs. (a) Schematic showing cleavage of MBP tags from MBP-Nup100 and MBP-Nsp1. TEV-protease was added to the hybridization reaction and held at room temperature for 1.5 hours before purification of excess protein *via* rate-zonal centrifugation. (b) SDS-agarose and SDS-page gels of rate-zonal centrifugation fractions of NuPODs with Nup100. The uncleaved and unpurified reaction contained only the MBP-Nup100 construct. After purification, partially cleaved free proteins were collected in the early fractions and the Nup100-NuPOD construct in fraction 6. (c) As in b, with Nsp1.

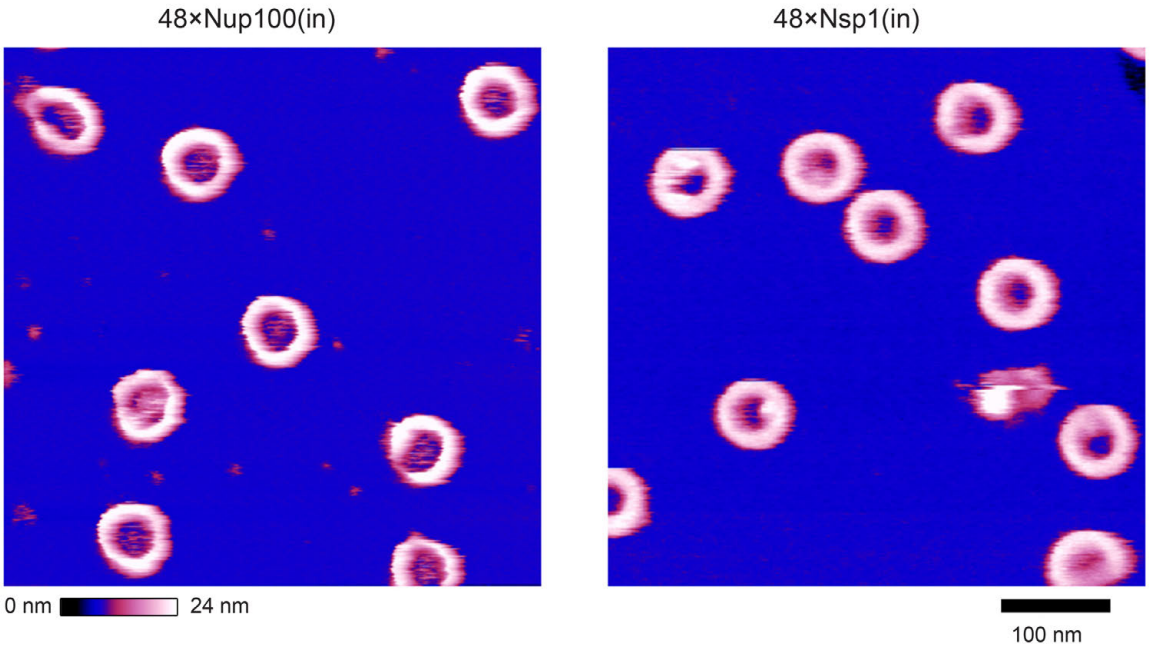

Figure S12. AFM images of NuPODs after MBP tag removal. Tapping mode AFM images of 48×Nup100(in) and 48×Nsp1(in) NuPODs deposited on lipid bilayers after MBP tag cleavage.

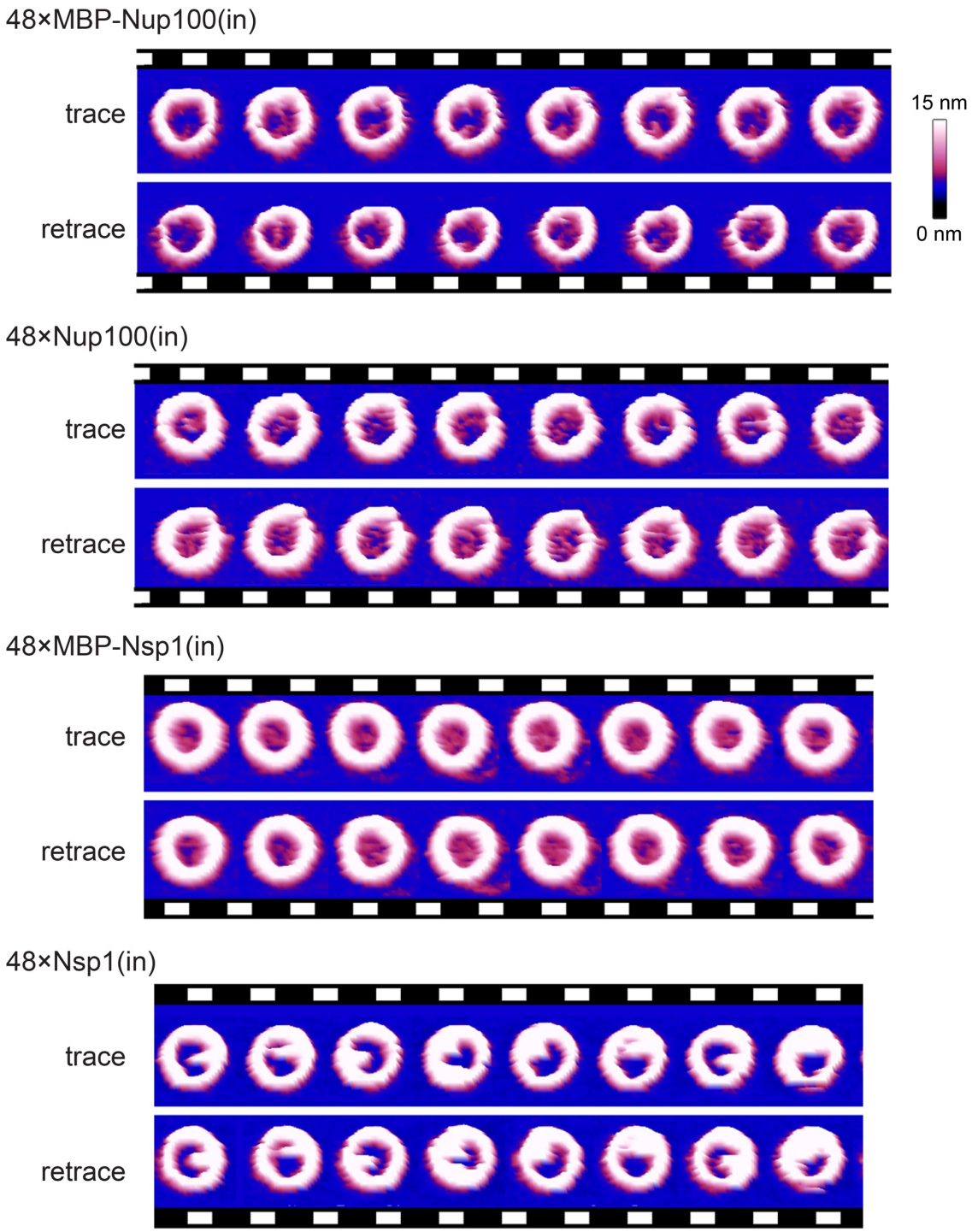

Figure S13. Validating robustness of time-resolved AFM imaging of NuPODs. Comparison of trace (as displayed in Figure 5a) and retrace of a NuPOD containing 48×MBP-Nup100(in), 48×Nup100(in) with MBP cleaved off, 48×MBP-Nsp1(in), and 48×Nsp1(in) with MBP cleaved off, with 1.6 s between subsequent scans. Features that reproduce between trace and retrace images (see SI extended methods) can be attributed to changes in the sample, as opposed to noise in the measurement.

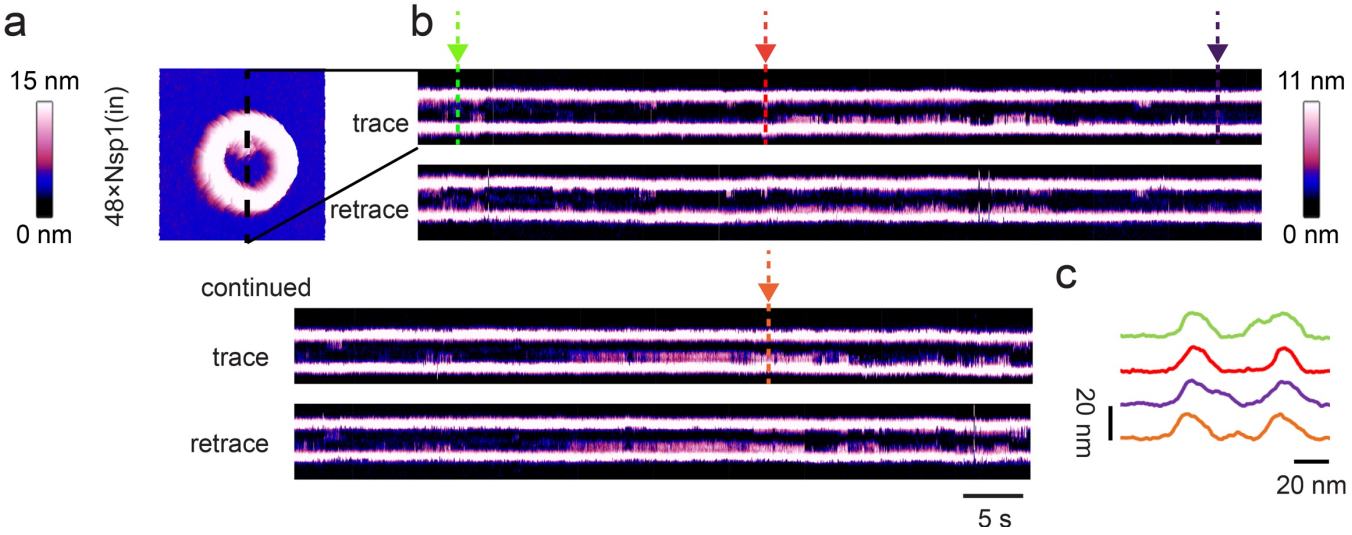

Figure S14. Time-resolved imaging of FG-nup dynamics within NuPODs reveal transient molecular interactions. (a) AFM image of an inside-grafted 48×Nsp1(in) NuPOD with MBP cleaved off. The dashed line indicates where height profiles were recorded (on this same NuPOD) for the kymographs in b. (b) Kymographs showing the AFM height profile across the NuPOD as a function of time, with trace (top) and retrace (bottom) shown separately to validate the robustness of the observed fluctuations, and with 50 ms between subsequent scan lines. (c) Height profiles along positions indicated in b. Color scale, 0–15 nm (a), 0–11 nm (b).

Table S1. Amino acid sequence of constructs used in this study. FG-domains (Nup100 2-610 and Nsp1 2-603) are in black text, his tag in blue text, and all other features in grey text. Negatively charged residues (D/E) are underlined in blue, positively charged residues (R/K) in red. GLFG repeats are highlighted in yellow, FxFG in red, other FGs in grey (including 2 FXFX repeats in Nsp1). C-terminal cysteine residues are highlighted in cyan.

MBP-SUMO-Cys	1 MGHHHHHHHHHHKIEEGKLVIWINGDKGYNGLAEVGKKFEKDTGIKVTVEHPDKLEEKFP 61 QVAATGDGPDIIFWAHDRFGGYAQSGLLAEITPDKAFQDKLYPFTWDAVRYNGKLIAYPI 121 AVEALSLIYNKDLLPNPPKTWEEIPALDKELKAKGKSALMFNLQEPYFTWPLIAADGGYA 181 FKYENGKYDIKDVGVDNAGAKAGLTFLVDLIKNKHMNADTDYSIAEAAFNKGETAMTING 241 PWAWSNIDTSKVNYGVTVLPTFKGQPSKPFVGVLSAGINAASPNKELAKEFLENYLLTDE 301 GLEAVNKDKPLGAVALKSYEEELAKDPRIAATMENAQKGEIMPNIPQMSAFWYAVRTAVI 361 NAASGRQTVDEALKDAQTASMSDSEVNQEAKPEVKPEVKPETHINLKVSDGSSEIFFKIK 421 KTTPLRRLMEAFAKRQGKEMDSLRFLYDGIRIQADQTPEDLDMEDNDIIEAHREQIGGSE 481 FELRRQACGRTRAPPPPPLRSGC
MBP-SUMO-TEV-Nup100 2-610-Cys	1 MGHHHHHHHHHHKIEEGKLVIWINGDKGYNGLAEVGKKFEKDTGIKVTVEHPDKLEEKFP 61 QVAATGDGPDIIFWAHDRFGGYAQSGLLAEITPDKAFQDKLYPFTWDAVRYNGKLIAYPI 121 AVEALSLIYNKDLLPNPPKTWEEIPALDKELKAKGKSALMFNLQEPYFTWPLIAADGGYA 181 FKYENGKYDIKDVGVDNAGAKAGLTFLVDLIKNKHMNADTDYSIAEAAFNKGETAMTING 241 PWAWSNIDTSKVNYGVTVLPTFKGQPSKPFVGVLSAGINAASPNKELAKEFLENYLLTDE 301 GLEAVNKDKPLGAVALKSYEEELAKDPRIAATMENAQKGEIMPNIPQMSAFWYAVRTAVI 361 NAASGRQTVDEALKDAQTASMSDSEVNQEAKPEVKPEVKPETHINLKVSDGSSEIFFKIK 421 KTTPLRRLMEAFAKRQGKEMDSLRFLYDGIRIQADQTPEDLDMEDNDIIEAHREQIGGHM 481 ENLYFQGFGNNRPMFGGSNLSFGSNTSSFGGQQSQQPNSLFGNSNNNNNSTSNNAQSGFG 541 GFTSAAGSNSNSLFGNNNTQNNGAFGQSMGATQNSPFGSLNSSNASNGNTFGGSSSMGSF 601 GGNTNNAFNNNSNSTNSPFGFNKPNTGGTLFGSQNNNSAGTSSLFGGQSTSTTGTFGNTG 661 SSFGTGLNGNGSNIFGAGNNSQSNTTGSLFGNQQSSAFGTNNQQGSLFGQQSQNTNNAFG 721 NQNQLGGSSFGSKPVGSGSLFGQSNNTLGNTTNNRNGLFGQMNSSNQGSSNSGLFGQNSM 781 NSSTQGVFGQNNNQMQINGNNNNSLFGKANTFSNSASGGLFGQNNQQQGSGLFGQNSQTS 841 GSSGLFGQNNQKQPNTFTQSNTGIGLFGQNNNQQQQSTGLFGAKPAGTTGSLFGGNSSTQ 901 PNSLFGTTNVPTSNTQSQQGNSLFGATKLTNMPFGGNPTANQSGSGNSLFGTKPASTTGS 961 LFGNNTASTTVPSTNGLFGNNANNSTSTTNTGLFGAKPDSQSKPALGGGLFGNSNSNSST 1021 IGQNKPVFGGTTQNTGLFGATGTNSSAVGSTGKLFGQNNNTLNVGTQNVPPVNNTTQNAL 1081 LGTTAVPSLQQAPVTNC
MBP-SUMO-TEV-Nsp1 2-603-Cys	1 MGHHHHHHHHHHKIEEGKLVIWINGDKGYNGLAEVGKKFEKDTGIKVTVEHPDKLEEKFP 61 QVAATGDGPDIIFWAHDRFGGYAQSGLLAEITPDKAFQDKLYPFTWDAVRYNGKLIAYPI 121 AVEALSLIYNKDLLPNPPKTWEEIPALDKELKAKGKSALMFNLQEPYFTWPLIAADGGYA 181 FKYENGKYDIKDVGVDNAGAKAGLTFLVDLIKNKHMNADTDYSIAEAAFNKGETAMTING 241 PWAWSNIDTSKVNYGVTVLPTFKGQPSKPFVGVLSAGINAASPNKELAKEFLENYLLTDE 301 GLEAVNKDKPLGAVALKSYEEELAKDPRIAATMENAQKGEIMPNIPQMSAFWYAVRTAVI 361 NAASGRQTVDEALKDAQTASMSDSEVNQEAKPEVKPEVKPETHINLKVSDGSSEIFFKIK 421 KTTPLRRLMEAFAKRQGKEMDSLRFLYDGIRIQADQTPEDLDMEDNDIIEAHREQIGGHM 481 ENLYFQGNFNTPQQNKTPFSFGTANNNSNTTNQNSSTGAGAFGTGQSTFGFNNSAPNNTN 541 NANSSITPAFGSNNTGNTAFGNSNPTSNVFGSNNSTTNTFGSNSAGTSLFGSSSAQQTKS 601 NGTAGGNTFGSSSLFNNSTNSNTTKPAFGGLNFGGGNNTTPSSTGNANTSNNLFGATANA 661 NKPAFSFGATTNDDKKTEPDKPAFSFNSSVGNKTDAQAPTTGFSFGSQLGGNKTVNEAAK 721 PSLSFGSGSAGANPAGASQPEPTTNEPAKPALSFGTATSDNKTTNTTPSFSFGAKSDENK 781 AGATSKPAFSFGAKPEEKKDDNSSKPAFSFGAKSNEDKQDGTAKPAFSFGAKPAEKNNNE 841 TSKPAFSFGAKSDEKKDGDASKPAFSFGAKPDENKASATSKPAFSFGAKPEEKKDDNSSK 901 PAFSFGAKSNEDKQDGTAKPAFSFGAKPAEKNNNETSKPAFSFGAKSDEKKDGDASKPAF 961 SFGAKSDEKKDSDSSKPAFSFGTKSNEKKDSGSSKPAFSFGAKPDEKKNDEVSKPAFSFG 1021 AKANEKKESDESKSAFSFGSKPTGKEEGDGAKAAISFGAKPEEQKSSDTSKPAFTFGAQK 1081 DNEKKTEESC

Table S2. Copy number of MBP-Nup100 in NuPODs. Immunoblots of samples normalized by DNA concentration were compared to an internal standard curve of MBP-Nup100, and quantities were interpolated using a quadratic fit in GraphPad Prism. Protein quantity was then converted to copies per NuPOD. N is number of separate blots (with separate internal standard curves).

Sample	Mean	SD	N
1×MBP-Nup100	1.1	0.1	4
8×MBP-Nup100	7.0	2.0	4
16×MBP-Nup100	16.6	6.8	5
24×MBP-Nup100	24.5	11.3	5
32×MBP-Nup100	30.0	11.0	5
48×MBP-Nup100	45.1	5.2	5